THE UNIVERSITY OF MICHIGAN

INDUSTRY PROGRAM OF THE COLLEGE OF ENGINEERING

THE ROLE OF THE SOLID-LIQUID INTERPHASE BOUNDARY IN MICROSTRUCTURES

Otto K. Riegger

October, 1962

IP-584

ACKNOWLEDGEMENTS

It is a pleasure for the author to acknowledge a number of individuals and organizations who provided indispensible assistance during the course of this investigation. Professor Lawrence H. Van Vlack, Chairman of the Doctoral Committee, stimulated interest in the topic, provided much encouragement through the experimental stages, and made himself ever available for consultation.

Professor Edward E. Hucke provided stimulating critical discussions on the interpretation of some of the results. The other members of the Doctoral Committee provided assistance through their interest and cooperation.

The author is indebted to the shop personnel of the Department of Chemical and Metallurgical Engineering for their aid with equipment and to Mr. Frank Drogosz for his suggestions on equipment and repairs. The faculty and many fellow graduate students provided aid through discussions and assistance with experimental programs. In particular, the author expresses his thanks to Mr. Gerald I. Madden who helped with much of the metallographic work and to Mr. Charles Stickels who wrote the program for processing the data on the computer.

The Wheelabrator Corporation and the General Electric Company provided the author with fellowships through part of his graduate work. The author expresses his thanks to Miss Dolores Gillies, who typed the first draft and to the Industry Program of the College of Engineering, which prepared the dissertation in its final form.

Finally, the author expresses his gratitude for the patience and encouragement of his wife and parents throughout the course of this investigation.

TABLE OF CONTENTS

TABLE OF CONTENTS CON'D

LIST OF TABLES

LIST OF FIGURES

LIST OF FIGURES CONT'D

ABSTRACT

This investigation is concerned with a study of the inter-relationship between temperature and phase composition on the phase distribution in equilibrated microstructures. The systems chosen for study included: (1) single phase molybdenum metal, (2) several liquid inclusions in equilibrium with solid nickel and with solid silicon metals, (3) various liquids in equilibrium with the intermetallic compounds AlSb, Sn Te, and Mg_3Sb_2, and (4) various oxide liquids in equilibrium with solid periclase (MgO). The microstructures obtained in the different systems are described and changes in them are related to the changes in composition and/or ordering in the liquid phase.

The metallic and intermetallic compound samples were prepared by induction melting appropriate quantities of high purity metals and subsequent heat treating at selected temperatures produced the equilibrated microstructures. An exception to this procedure was molybdenum metal which was equilibrated by high temperature annealing of a previously cold drawn wire. Periclase (MgO) samples were prepared by sintering appropriate quantities of premixed and pressed powders of the various oxides at selected temperatures. Standard polishing procedures, followed by etching for contrast between phases when necessary, were used in preparing sample sections for metallographic examination. The analysis involved measuring a number of randomly selected dihedral angles formed by the quenched liquid phase between two solid grains at the grain boundary between them. Grain diameters were also measured in the periclase (MgO) materials.

The modified angle measuring and data processing techniques were validified by giving the expected value of 120° for the true dihedral angle in a well-annealed molybdenum single phase microstructure.

A change in microstructure accompanying a change in temperature was found to occur only when the change in temperature produced a substantial change in the solubility of the solid in the liquid for the wide variety of metallic and intermetallic compound forming systems studied. The change in microstructure was detected through the dihedral angle which is in turn controlled by the ratio of the solid/liquid interface energy to the grain boundary energy. A correlation between this ratio and the logarithm of the solubility of the solid in the liquid is found to hold within a given two phase region for the metallic and intermetallic compound forming systems studied. Indications that an "ordered" liquid can form a low energy solid/liquid are found in all of the intermetallic compound forming systems studied. The composition of the liquid phase is found to have only a secondary effect on the microstructures containing the solid periclase (MgO).

The effect of interfacial free energy as a driving force for grain growth is found in both solid-liquid microstructures containing intermetallic compounds as the solid phase, and periclase (MgO) as the solid phase. The rate of grain growth of periclase (MgO) was found to increase markedly with increases in temperature.

CHAPTER I

INTRODUCTION

This investigation is concerned with a study of the inter-relationship between temperature and phase composition on the phase distribution in equilibrated solid-liquid microstructures. The microstructures of metals have been widely studied with respect to the geometry and shape of the individual crystallites in a poly-crystalline material. The rates of grain growth at constant temperature and their variation with temperature have also received much attention. A number of studies have also been centered around the geometry and distribution of a second phase in metallic systems. The second phase may be either solid or liquid and may have its origin in trace impurities such as sulfur in iron or bismuth in copper. It may be an equilibrium microconstituent such as carbides in steel or alpha-beta brasses, or it may result from the intentional modification of impurities to a more harmless form such as the modification of surfur and bismuth by manganese and phosphorus in iron and copper respecitvely. The microstructures revealed by these studies have formed the bases of explanations as to why some impurities have a deleterious effect on physical properties and why some additives modify these harmful effects. Thus, the fact that microstructures play an important role in determining physical properties in metals has been well established for some time.

In view of our knowledge in metallic systems and the inter-relationship between microstructures and properties, it was thought

that a study of the microstructures of other materials such as intermetallic compounds and oxides might prove to be interesting. These materials have received very little attention from the microstructural point of view, although they are becoming increasingly more important industrially. In addition to providing useful information which may be used to interpret and predict physical properties of materials, such a study could give some insight into the factors which control the geometry of phase distribution in microstructures. The systems chosen for study include:

1. Single phase molybdenum metal.
2. Several liquid inclusions in equilibrium with solid nickel and with solid silicon metals.
3. Various liquids in equilibrium with the intermetallic compounds AlSb, SnTe, and Mg_3Sb_2.
4. Various oxide liquids in equilibrium with solid periclase (MgO).

The single phase molybdenum was selected because it was thought to be well annealed and therefore had a known microstructure on which the measuring and analysis techniques could be checked. The nickel and silicon systems chosen are ones which formed simple binaries with interesting features in their liquidus contours.

The intermetallic compounds forming systems are of interest for two reasons. First, their binary diagrams show the unique feature of being able to have liquids of two different compositions in equilibrium with essentially the same solid at a constant temperature. Secondly, these materials are receiving more attention on a commercial basis because many possess unique semiconducting or thermoelectric properties, and for these applications one is also interested in physical properties.

The microstructures of periclase (MgO) base materials are of interest because of their important use as refractories in steel-making furnaces, and because commercial compositions are known to develop cracks in the presence of small amounts of an equilibrium liquid phase at temperatures far below the melting point of periclase (MgO).

The microstructures obtained in the different systems will be described and attempts to interpret and explain changes in microstructure will be based on changes in the composition and/or ordering of the liquid phase involved.

CHAPTER II

LITERATURE REVIEW

The literature which is important to the study and understanding of microstructures will be considered by grouping pertinent works under the following topics: (1) Influence of interfacial tensions on microstructures, (2) influence of microstructure on properties, and (3) theoretical treatments of interfacial and surface tensions.

1. Influence of Interfacial Tensions on Microstructure

Interfacial tension effects exert themselves in microstructures in two ways: first, they control the geometry or configuration of microstructural features, and secondly, they can exert a driving force which tends to increase the size of microstructural features. The second phenomenon is commonly termed grain growth.

Harker and Parker[1] studied the combined effects of interfacial tension on the microstructure of several single phase metals. They showed that, as a metal approached geometric equilibrium, the grain boundary junction angles approached 120 degrees. To do this, it was necessary to relate the geometric features seen on a two-dimensional polished section to the actual structures which occur in three-dimensional space. They were able to calculate the theoretical distribution of angles expected to be seen on the two-dimensional section for a structure in which only 120 degree angles exist between adjacent grain faces through the equation

$$\tan \psi = \frac{2 \sin x \cos \theta}{\sin^2\theta \, (\cos 2\phi - \cos x) + 2 \cos x} \qquad (1)$$

where $\underline{x}$ is the true dihedral angle, in this case 120 degrees, ψ is the angle observed on the two-dimensional section, and ϕ and θ are solid polar coordinates.

Later, Smith[2] showed that the idea of interfacial tensions could be applied to two-phase metallic systems, and that the geometric configurations established were the result of the system attempting to come to a state of lowest energy.

In particular, he has shown that the relation:

$$\gamma_{S/S} = 2\gamma_{S/L} \cos \frac{\theta}{2} \qquad (2)$$

is applicable in a microstructure which contains a solid and a liquid in equilibrium. In Equation (2), $\gamma_{S/S}$ is the grain boundary energy between two adjacent grains of the solid, $\gamma_{S/L}$ is the interface energy at the phase boundary between the solid grains and the liquid, and θ is the dihedral angle of penetration which the liquid makes between two solid grains. Three exemplary situations showing how the ratio of the phase boundary energy to the grain boundary energy controls the solid/liquid phase geometry are presented in Figure 1.

Smith also calculated theoretical distributions for true dihedral angles of 30, 60, 90 and 150 degrees and concluded that in every case the most frequently observed angle was within 5 degrees of the true angle. He was therefore led to interpret his experimental data on the basis of frequency plots. While this method is correct

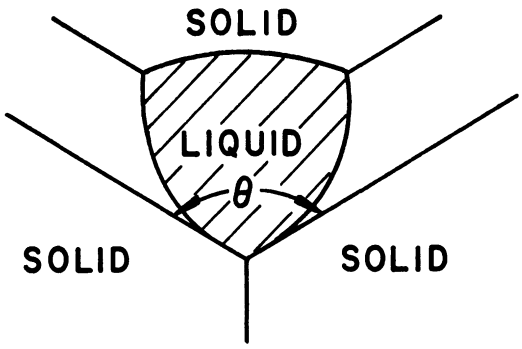

a) $\frac{\text{Phase Boundary Energy}}{\text{Grain Boundary Energy}} = 1; \quad \theta = 120°$

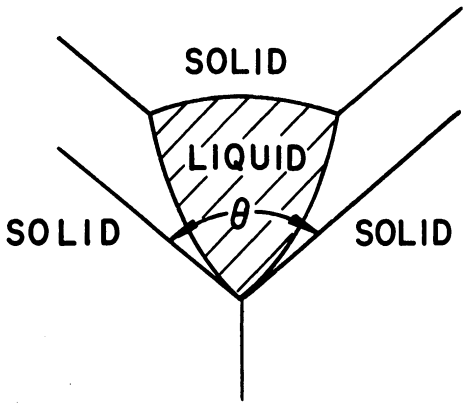

b) $1 > \frac{\text{Phase Boundary Energy}}{\text{Grain Boundary Energy}} > 0.5; \quad 120° > \theta > 0°$

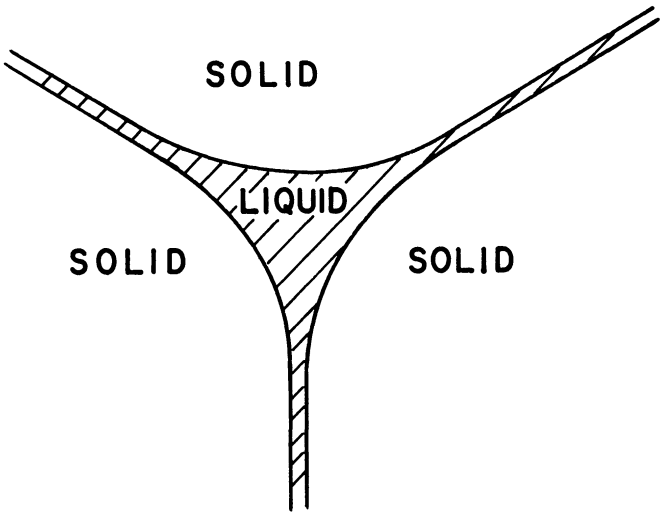

c) $\frac{\text{Phase Boundary Energy}}{\text{Grain Boundary Energy}} \leq 0.5; \quad \theta = 0°$ (i.e., continuous film)

Figure 1. Liquid Phase Distribution

in theory, it was found in practice that a large number (usually 250 to 500) of angles had to be measured to give a satisfactory value for the true dihedral angle.

Recently Riegger and Van Vlack[3] showed that the median angle of the calculated distribution for any angle (0 to 180 degrees) is within two degrees of the true angle. They found that in practice, the median angle (as opposed to the statistical mode as used by Smith) of a smaller number of measured angles will give a satisfactory value for the true dihedral angle.

By developing a stereoscopic microradiography technique, Williams and Smith[4] were able to study grain shapes in an aluminum-tin alloy. They found that the grains were closely analogous in shape to soap bubbles in a froth where surface tension and space-filling alone determine the structure. Only four percent of the grains studied were found to deviate from the simple surface tension type and these were thought to be caused either by grains going through the growing process or variations in grain boundary tension.

Smith and Ikeuye[5] studied the variations, with temperature and composition, of interfacial energy through their effect on microstructures in a number of metallic systems. They reported that the effect of temperature on the dihedral angle and the relative energies of the grain boundary and the interface boundary in copper-lead and aluminum-tin alloys is slight except when the change in temperature produces a change in the composition of the phases in equilibrium. It was predicted that, in general, alloys whose constitution diagrams show

a nearly vertical liquidus will be substantially unaffected by temperature changes, and that alloys with a sloping liquidus will present structures that vary considerably with annealing temperature. They also stated that the dihedral angle decreases as the composition of the liquid approaches that of the solid.

Van Vlack[6] studied the variations of the relative solid/liquid interface boundary energies in the iron-sulfur-oxygen system with changes in temperature and composition. He found that the relative energy of the liquid sulfide/iron interfaces decreased with increases in temperature. It was suggested that part of the decrease may be attributed to an increase in the iron content of the liquid to give a composition closer to that of the solid as predicted by the iron-sulfur phase diagram. Additions of oxygen to the sulfide were found to increase the relative energy of the liquid sulfide-oxide/iron interface and this increase was attributed to the fact that oxygen decreases the solubility of iron in the sulfide-oxide liquid.

Later, Van Vlack et al.[7] substantiated the work in the iron-sulfur-oxygen system and reported a number of observations in the iron-manganese-silicon-sulfur-oxygen system. With properly adjusted compositions, a solid iron phase, a solid manganese-sulfide phase, and a liquid silicate phase can exist in equilibrium. They found that the relative energy of the liquid silicate/iron interface compared to the iron/iron grain boundary was insensitive to temperature over a wide range. Over the same temperature range, however, the relative energy of the liquid silicate/manganese sulfide interface compared to the manganese sulfide grain boundary was found to decrease significantly.

Examination of the known phase relationships over this temperature range indicated that the solubility of iron in the silicate liquid was essentially constant, but that the solubility of manganese sulfide in the silicate liquid was greatly increased. These observations are in agreement with Smith's generalization[5] that the relative energy of the interphase boundary compared to the grain boundary, decreases as the composition of the liquid approaches that of the solid and that the effect of temperature is slight except when the change produces a change in the composition of the phases in equilibrium.

Van Vlack[8] has shown that the microstructure of silica in the presence of iron oxide liquids can be described in terms of the relative interfacial energies of the phase and grain boundaries. He found only a slight change in the relative energy of the liquid iron oxide/silica interphase energy with temperature. This behavior may be explained by the fact that there is little change in the solubility of the solid silica in the liquid over the temperature range studied. It was also found that the microstructures were unaffected by changes in the oxidation level and this was interpreted to be due to the fact that the molar fraction of silica in the liquid phase does not change significantly over the range of oxygen pressures studied.

It should be pointed out that in the discussion so far, the terms surface or interface tension and interfacial free energy have been used interchangeably. While Shuttleworth[9] has pointed out that the two quantities are not equal for solids at low temperatures, they approach each other at higher temperatures, and are numerically equal

for liquids. For our present considerations on microstructures involving grain boundaries and solid/liquid interface boundaries, the energy and the interface tension may be considered to be equal since the temperatures involved are above one-half of the melting point of the solid and the equilibrium involves a solid/liquid interface. A distinction between the two quantities will not be made because it will not influence the present results or interpretations.

The second influence of surface tensions on microstructures is that of being a driving force for grain growth. In a recent review paper on the subject, Fullman[10] has stated that "the primary driving force for grain growth is the decrease in grain boundary interfacial free energy that accompanies an increase in grain diameter." Beck, et al.[11] have suggested that the rate of grain growth would be proportional to the interfacial free energy per unit volume as given by the equation:

$$\frac{dD}{dt} = \frac{C\gamma}{D} \qquad (3)$$

where D is the average grain diameter, t the time of annealing, γ the interfacial free energy of the grain boundaries, and C a constant at any temperature. If we can assume that the interfacial free energy is constant, the integrated form of Equation (3) can be written as:

$$D^2 - D_o^2 = Bt \qquad (4)$$

where B is a constant. Fisher[12] has experimentally checked the validity of Equation (4) by showing that it well describes the growth

of bubbles in a two-dimensional soap froth where the structural geometry is controlled only by surface tension. In relatively pure metals, Equation (4) does not adequately describe the grain growth phenomenon in that the size does not increase with the square root of time but rather by some different exponent which varies with temperature and alloy composition. Among the various factors cited as being responsible for this deviation of the exponent are inclusions, changes in the grain boundary energy, adsorption in the grain boundary, orientation effects, polygonization, and strain.

Burke[13] has pointed out that the driving force for grain growth in ceramics is the surface tension of the grain boundaries and that Equation (4) adequately describes the phenomenon in these systems. Kingery[14] has shown that the driving force for the sintering process in the presence of a liquid phase is liquid/vapor surface energy and that densification is a consequence of the natural tendency to minimize the total surface energies and thereby reduce the interface areas.

Recently, Van Vlack and Riegger[15] have reported that the rate of grain growth magnesiowüstite in the presence of a silicate liquid is described by Equation (4), i.e., that the average magnesiowüstite grain size increases with the square root of time. This implies that the grain growth is controlled by the energies of the solid/liquid interphase boundary.

2. Influence of Microstructure on Properties

Metallurgists have long been engaged in the process of relating microstructures to physical properties. In particular, solid-liquid

microstructures have been related to a number of phenomena such as liquid metal embrittlement, hot shortness, high temperature properties, weld cracking, and many others.

The embrittling effect of bismuth on copper was recognized by Voce and Hollowes[16] and by Schofield and Cuckow[17] as being associated with a thin film of bismuth in the grain boundaries of the copper. It was also found that phosphorus eliminated brittleness by restricting the bismuth to small pockets at grain corners and did not allow a grain boundary film to form. Smith[2] has explained these findings in terms of relative interfacial tensions which control the geometry of liquid inclusions. From his theory, it would be expected that lead inclusions in copper would not have the embrittling effect on copper because the degree of penetration along grain boundaries is restricted to angles larger than 60 degrees. This speculation was substantiated by Kraai[18] who found that the strength of copper wires, tested in contact with liquid bismuth-lead alloys, increased progressively as the lead content of the alloy increased. The increase in strength was accompanied by an increase of the dihedral angle (or a decrease in the degree of grain boundary penetration by the liquid alloy) as the composition of the liquid alloys increased progressively from pure bismuth to pure lead.

Hot shortness in steels has been attributed by Sims and Lilliequist[19], and by Benedicts and Lofquist[20], to the fact that, in the absence of manganese, any sulfur present will be in the form of iron sulfide which tends to form a continuous network in the grain boundaries of the primary iron grains. Later, Van Vlack, et al.[7]

interpreted the microstructures of various iron-sulfur-alloy systems on the basis of the relative interfacial energies of the boundaries involved and related them to known compositions which are subject to the hot shortness phenomenon.

Recently Van Vlack[8] has described the microstructures developed by silica in the presence of an iron oxide liquid in terms of interfacial energy relations. He attributed the strength which silica refractories retain at high temperatures in the presence of high liquid contents, to these energy relations which allow the structure to maintain a considerable amount of solid-to-solid contact. This contact is maintained because the liquids do not penetrate the silica grain boundaries extensively. On the other hand, Van Vlack and Riegger[15] have found that siliceous liquids completely penetrate the grain boundaries in magnesiowüstite solids. A similar distribution of a silicate liquid was reported by Wells and Van Vlack[21] for commercial periclase refractories studied after they had been in service in steel-making furnaces. The formation of cracks under load conditions was attributed to the weakening of the structure due to the extensive liquid penetration.

Borland[22] has recently suggested an explanation of hot cracking in steel welds based on microstructures and has related the extent to which it occurs to the distribution of a liquid phase developed as a result of impurity elements after the primary iron has solidified. He has shown that changes in composition play an important part in changing the distribution of the liquid phase, and thereby alter the cracking tendency.

3. Theoretical Treatments of Interfacial and Surface Tension

A comprehensive theoretical development for treating the phenomena of surface tension by the methods of thermodynamics has been presented by Gibbs[24] in his treatise on heterogeneous equilibrium. This theory was recently reviewed by Tolman[23]. One of the most important consequences of this theory is the expression, derivable therefore, for the dependence of the surface tension on the temperature and the chemical potential of the components. The expression for a two-phase system may be written:

$$-d\gamma = SdT + \Gamma_1 d\mu_1 + \Gamma_2 d\mu_2 \qquad (5)$$

where γ is the surface tension, S is the entropy of the interface material per unit area, T the absolute temperature, μ the chemical potential, and Γ_i the excess amount of component i at the interface. This expression is commonly called the Gibbs adsorption equation. The excess is defined by Gibbs[24] as the difference per unit area of boundary between the actual number of atoms of a component in a system and the number that would have been present in the same volume if the material on each side of the boundary had remained unchanged up to an imaginary dividing surface.

In a similar treatment, Guggenheim[25] has introduced two dividing surfaces, one on each side of the boundary, and the Γ's are defined as the total number of moles per unit area in the material between the two dividing surfaces. Because of the Gibbs-Duhem relation Equation (5) holds true for either definition.[26]

Cahn and Hilliard[26] have made use of the Gibbs adsorption equation to calculate the maximum amount of equilibrium segregation of phosphorus which can occur in the grain boundaries of iron. To do this, it was necessary to assume that a grain boundary tension exists which is not seriously variable with orientation of the solid grains. Using the same assumptions, Cahn and Hilliard[27] were able to calculate an estimate for the minimum number of atoms that must be associated with a unit area of grain boundary in the copper-gold system. Making some reasonable assumptions about the structure and density of the grain boundary, they were able to show that the interface excesses given by Equation (5) could be accomodated in a monolayer.

Taylor[28] has applied the Gibbs adsorption equation to Ikeuye and Smith's[5] data for alloys in the aluminum-tin-X systems (X = bismuth, lead, or cadimum), and has concluded that it adequately describes the changes of the solid/liquid interfacial energies with solubility. It appears to the present author that he might have taken some liberties in smoothing the data before making the correlation, however, it is apparent that a definite trend exists, as Taylor postulated.

Skapski[29] has calculated the temperature coefficient of the surface tension of liquid metals from an approach based on the concept of a "structure" of liquids. The influence of temperature is expressed as the difference in entropy of atoms situated in the surface and atoms in the bulk, which is estimated from assumptions about the configuration of nearest neighbors. Two entropy terms are considered. One accounts

for the difference in the frequency of oscillation and the second for the difference in configuration of atoms inside the bulk and on the surface. The temperature coefficients are all negative, however, they are lower than experimental values reported by Allen and Kingery[30] for a number of pure metals over wide temperature ranges.

A theory of the surface tension of solids based on the coordination of nearest neighbors has also been developed by Skapski[31]. It allowed him to calculate the solid surface tensions of gold, silver, and copper and these were found to be in good agreement with experimental values determined by the thin foil or wire stretching methods. The theory also allowed him to calculate the solid/liquid interface energy of a solid with its own liquid at the melting-point, and these values were found to compare favorably with those determined by Turnbull from experiments of undercooling small metal droplets. However, Hilliard and Cahn[32] have raised serious questions about the values obtained by Turnbull. They concluded that there is some degree of diffuseness at the solid/liquid interface, and that the diffuseness is such that the values of solid/liquid interface energy estimated from the undercooling experiments are too low because the liquid droplets were so small that any diffuseness in the boundary could not be tolerated.

Using as a basis the theoretical development of Schuschowitzky and Guggenheim, Taylor[33] has calculated the surface tensions of binary liquid-alloy mixtures. Good agreement was obtained between the calculated and experimental surface tension-composition relationships in simple eutectic systems, while considerable discrepancies were found for systems

showing intermediate phase formation in the solid state. This condition led to calculated values which were much higher than the experimental ones. It was suggested that in these compound forming systems, the surface does not have the simple monolayer structure assumed in the analysis.

CHAPTER III

EXPERIMENTAL PROCEDURE

1. Sample Preparation - Metals and Intermetallic Compounds

Small ingots of the desired alloy were prepared by melting appropriate quantities of high purity metals in an induction coil. The chemical analyses of the materials used are given in Table I. The melts were contained in, and allowed to solidify in crucibles made of either spectroscopic grade graphite or Morganite's recrystallized alumina. The melting arrangement is shown in Figure 2. Melting was carried out under an inert atmosphere of tank argon. The system was initially evacuated and refilled with argon several times before refilling to approximately atmospheric pressure for melting.

The nickel-bismuth, silicon-tin, and silicon-aluminum alloys were melted in recrystallized alumina crucibles. The aluminum-antimony, magnesium-antimony, and aluminum-antimony-indium alloys were melted in spectroscopic grade graphite crucibles. Alloys in the tin-tellurium system were melted in both types of crucibles.

The as-solidified ingots were sectioned and examined for homogeneity of the alloy distribution. The inclusion content was measured on a series of tin-tellurium alloys by a point counting technique. Measurements were made on cross sections from both the top and bottom of the ingots. The results of these measurements are tabulated in Table II. From these, it was concluded that the ingots in question were sufficiently homogeneous. With the exception of alloys in the aluminum-antimony-indium system, all other ingots were adjudged to be

TABLE I

ANALYSIS OF METALS USED FOR ALLOY PREPARATION*

Material		Electro Nickel	High Purity Bismuth	Silicon	High Purity Aluminum	High Purity Antimony	High Purity Tin	High Purity Tellurium	High Purity Indium	Sublimed Magnesium
Element	Cobalt	750	---	---	---	---	---	---	---	---
	Antimony	---	---	---	---	99.999+%	< 1	---	---	---
	Magnesium	---	---	---	20	0.1	0.1	1.0	---	99.9+%
	Lead	9	0.5	---	---	0.2	0.5	< 1.0	1.0	5.0
	Tin	---	---	---	---	0.5	99.999+%	---	3.0	---
	Silicon	---	---	99.8%	30	0.1	2.0	< 1.0	---	100
	Iron	9	0.5	---	10	0.2	0.3	< 1.0	< 1.0	7.0
	Nickel	99.89%	---	---	---	---	---	---	---	< 3.0
	Zinc	---	---	---	---	---	---	---	---	100
	Bismuth	---	99.999+%	---	---	1.0	0.1	---	---	---
	Aluminum	---	---	---	99.99+%	0.1	0.1	---	---	3.5
	Calcium	---	---	---	---	---	0.2	---	---	---
	Arsenic	---	---	---	---	3.0	---	---	---	---
	Copper	---	1.0	---	10	< 0.1	0.5	< 1.0	< 0.5	< 1.0
	Indium	---	---	---	---	---	0.5	---	99.999+%	---
	Cadenium	---	---	---	---	---	---	---	2.0	---
	Tellurium	---	---	---	---	---	---	99.999+%	---	---
	Silver	---	1.0	---	---	---	---	---	< 1.0	---
	Boron	10	---	---	---	0.1	0.2	---	---	---
	Hydrogen	3	---	---	---	---	---	---	---	---
	Oxygen	30	---	---	---	---	---	---	---	---
	Sulfur	10	---	---	---	---	---	---	---	---

* Parts per million, except for major element.

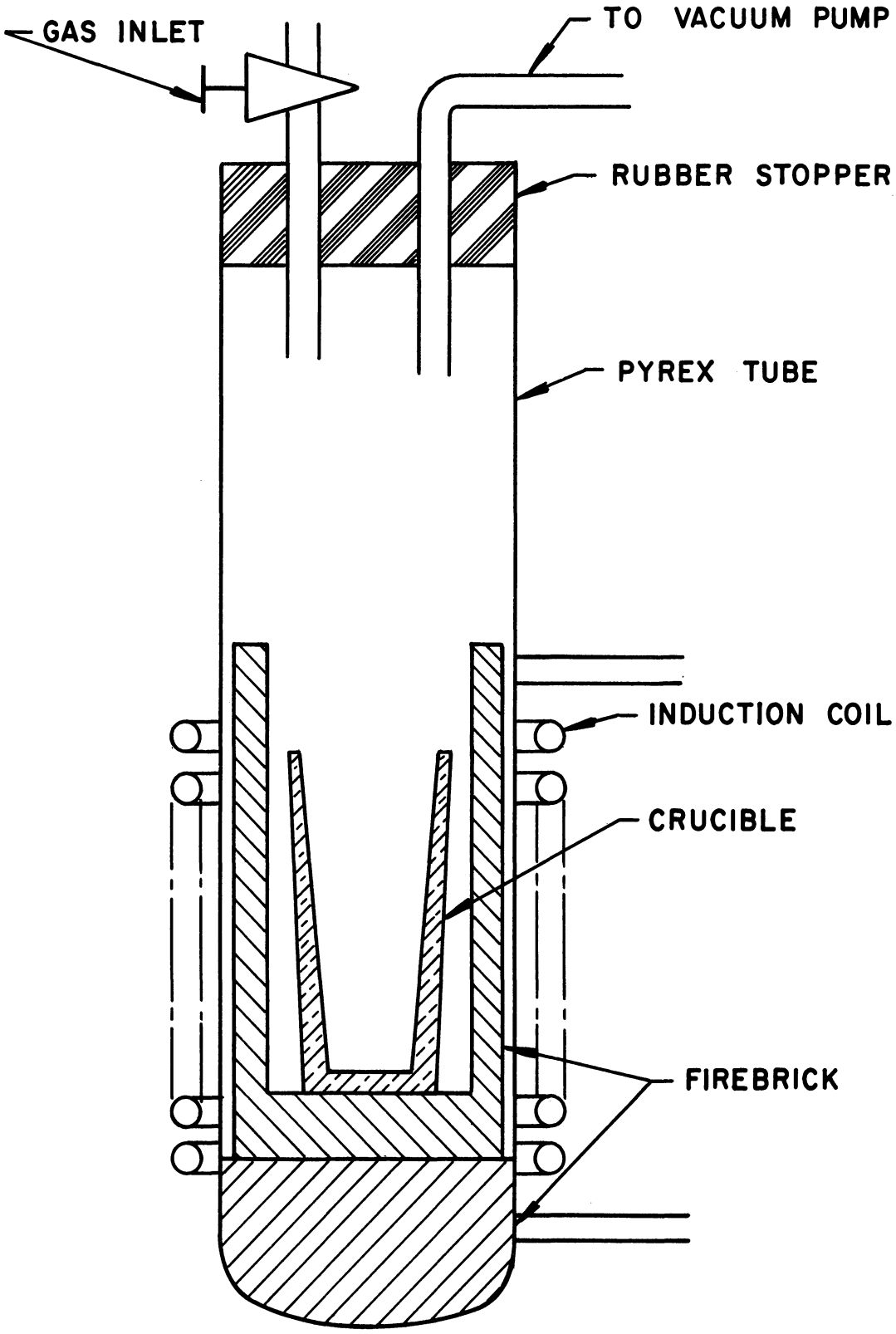

Figure 2. Controlled Atmosphere Melting Arrangement.

homogeneous by visual examination of the as-solidified structures.

Small sections were cut from the as-solidified ingots for heat treating in order to obtain geometric equilibrium at selected temperatures.

TABLE II

LIQUID CONTENT OF AS-SOLIDIFIED TIN-TELLURIUM ALLOYS

Sample Number	Aim Composition	Percent Liquid Top	Bottom
R-4	45% Sn - 55% Te	7.45	---
R-5	42.5% Sn - 57.5% Te	8.50	8.55
R-6	40% Sn - 60% Te	21.5	21.8
R-7	42.5% Sn - 57.5% Te	13.2	13.5

These samples were placed in a vycor tube, one end of which was closed and the other end was fitted with a ground glass joint and a stop cock. The vycor tube was evacuated and refilled with tank argon several times before finally refilling it to a pressure which would produce approximately one atmosphere of pressure at the heat-treating temperature. The heat treating was done in a small tube furnace which was heated by a chromel resistance winding. The temperature was controlled with a chromel-alumel thermocouple placed close to the furnace winding, which in turn fed output to a Foxboro potentiometer controller. Sample temperatures were measured by a separate chromel-alumel thermocouple placed outside the vycor tube but very close to the sample. At the end of an equilibration run, the tube was opened at the ground glass

joint and the sample quenched as rapidly as possible. For most alloys, quenching into still water gave satisfactory results. With the tellurium-rich tin-tellurium alloys, however, it was necessary to use a mixture of alcohol and dry ice in order to remove the heat fast enough so as to retain the high temperature structure of the solid-liquid alloy.

2. Sample Preparation - Oxides

Samples were made by sintering pellets pressed from the powders of the oxides. Reagent grades of magnesium oxide, calcium oxide, aluminum oxide, silicon dioxide, and iron oxide powders were used. Calculated amounts of the various powders were weighed out and carefully mixed to give the desired overall composition. Small pellets, 3/8 inch diameter by 1/4 inch thick were pressed from the mixed powders in a hardened steel die. For temperatures of 1600°C and below, the pellet samples were sintered in a Leco tube furnace equipped with silicon carbide resistance heating elements. The temperature was controlled with a platinum--platinum-rhodium thermocouple placed close to the heating elements, which in turn fed output to a Wheelco on-off controller. Sample temperatures were measured with a separate platinum--platinum-rhodium thermocouple placed in the furnace tube close to the samples. It is estimated that the sample temperature was maintained within ± 5°C of the reported sintering temperature. The pellet samples were placed in alumina boats lined with 0.003 inch platinum or platinum-20% rhodium sheet. Thus the samples could be moved in and out of the furnace and also prevented

their contamination from the boat material. Both ends of the furnace were open so that the samples were equilibrated under an atmosphere of air. At the end of a treating period, the boat containing the samples was pulled from the furnace as rapidly as possible and water-quenched in order to preserve the high temperature structure.

At temperatures of 1700 and 1800°C, the pellet samples were sintered in an oxy-acetylene fusion test furnace manufactured by the R. C. Remmey and Son Company. Oxidizing atmospheres were maintained by burning excess oxygen with the gas. The pellet samples were placed in alumina boats lined with 0.003 inch platinum - 20% rhodium and 0.005 inch platinum - 40% rhodium for runs at 1700 and 1800°C respectively. Temperatures were measured by sighting directly on the samples with an optical pyrometer. Temperatures were read at three to four minute intervals and the gas flow rates were adjusted manually to maintain the desired temperature. It is estimated that the sample temperature was maintained within $\pm$15°C of the reported sintering temperature. It was not possible to quench from these temperatures with the furnace arrangement used, however, it was noted that the samples lost 200 to 300°C of temperature within one to two minutes of shutting off the gas. It is doubtful that this slight delay in cooling through the solidus temperature materially altered the grain size as reported in the next chapter on results.

3. Sample Analysis

After the samples had been geometrically equilibrated by appropriate heat treating cycles, the analysis involved: (1) metallographically preparing a sample section for observation under the

microscope, and (2) making appropriate measurements on this section.

Samples were rough polished on 120, 400, and 600 grit wet silicon carbide papers after they had been mounted. Care was taken to remove 0.040 inch from the surface on the 120 grit paper. This insured that the bulk material was being examined, as the surface layer is often depleted in liquid content and may be subject to oxidation or other surface effects. Final polishing was done on five-micron and one-micron diamond wheels. In some instances it was desirable to polish further by hand on a Linde "B" wheel or mechanically on a Linde "B" Syntron. For a number of systems it was necessary to select an etchant or stain that would give contrast between the solid and quenched liquid phases. The etchants used are identified with the photomicrographs in the next chapter on results.

Measurements made on the polished section included the dihedral angle formed by the quenched liquid phase between two solid grains at the grain boundary between them, and grain diameters in the case of the magnesium oxide materials. Dihedral angles were measured by noting the amount of rotation of the stage of a Bausch and Lomb metallograph upon successively aligning both edges of angular inclusion with the cross-hair of a Filar eyepiece. All angle measurements were made at a magnification of 1000 diameters. Angles to be measured were selected on a random basis. Randomness on samples containing a large number of inclusions was obtained by moving the stage laterally without observation, and then measuring the inclusion which was closest to the cross-hair. On coarser structures, randomness was obtained by

measuring all the angles which were encountered along a random line or traverse of the sample. Only inclusions which showed definite interfacial angles were measured. Individual angle measurements were found to be reproducible to within about $\pm 1°$ for an angle of 30°. The error of measurement increased with increasing angle and is estimated to be $\pm$ 3° for an angle of 80°. The increase in error is due to the fact that liquid inclusions usually form curved interfaces with solids and the measuring technique involves placing a line tangent to this curved interface.

In the case of a single solid phase material, such as molybdenum, the grain boundary traces are close to being straight lines, and the reproducability of the angle measurements is estimated to be $\pm$ 1°, even though the true dihedral angle is approximately 120°. A more detailed discussion of measuring dihedral angles is given in Appendix A.

Grain sizes were determined on the magnesium oxide materials by measuring the diamter of a number of randomly chosen grains with a Filar eyepiece which had been calibrated against a grid of known spacing. Since the observations were made on a two-dimensional section, the average diameter reported will be smaller than the true average diameter by a factor of approximately 0.86.[34] However, the average diameter gives a consistent index for comparing the grain sizes of similar microstructures.

CHAPTER IV

EXPERIMENTAL RESULTS

For clarity in presentation, the systems studied in this investigation will be discussed in the order of their complexity, starting with the simplest and proceeding to the more complex. It should be point out, however, that this is not necessarily the order in which the most thorough investigations were conducted. Results will be presented under the headings of phase geometry and grain growth.

1. Phase Geometry in Microstructures

A. Single Phase Molybdenum Metal

It was thought desirable to check the measuring techniques and method of handling the experimental data by measuring dihedral angles on a sample where the true dihedral angle is thought to be known. This situation would be expected to be found in any well annealed single phase pure metal, in which grain boundary traces are expected to meet at angles of 120°.[1] Dihedral angles were therefore measured on a piece of molybdenum wire which had been cold drawn prior to annealing in a hydrogen atmosphere at approximately 1700°C for about 30 days. Measurements were made on both a cross-section and a longitudinal section in an area adjacent to where the wire had gone to a single crystal under the influence of a higher temperature. A summary of the angle results is given in Table III.

TABLE III

SUMMARY OF MOLYBDENUM ANGLE DATA

Number of Angles	Location	True Dihedral Angle (Degrees)	Fit Parameter
150	Cross section	120	3.59
150	Longitudinal section	119	3.63

The value of the true dihedral angle was determined using a least squares fitting technique to a theoretical curve calculated from Equation (1). The calculating and curve fitting were done on the IBM 709 computer using a program developed by Mr. Charles Stickels. The fit parameter is an indication of whether or not the distribution of measured angles is in close agreement with the theoretical distribution calculated. It is felt that a fit parameter of less than 5.00 means that the agreement is as good as one would expect for experimental data. An indication of this fit is shown in Figure 3 which is a plot of the first 50 data points from the cross section data.

Although the calculations were carried out to a greater degree of accuracy, the values reported for the true dihedral angle have been rounded off to the nearest degree. It is felt that reporting any greater accuracy is not warranted because the measuring was not this accurate and very little further information or meaning can be derived from the data. Microstructures of the molybdenum sample are shown in Figure 4.

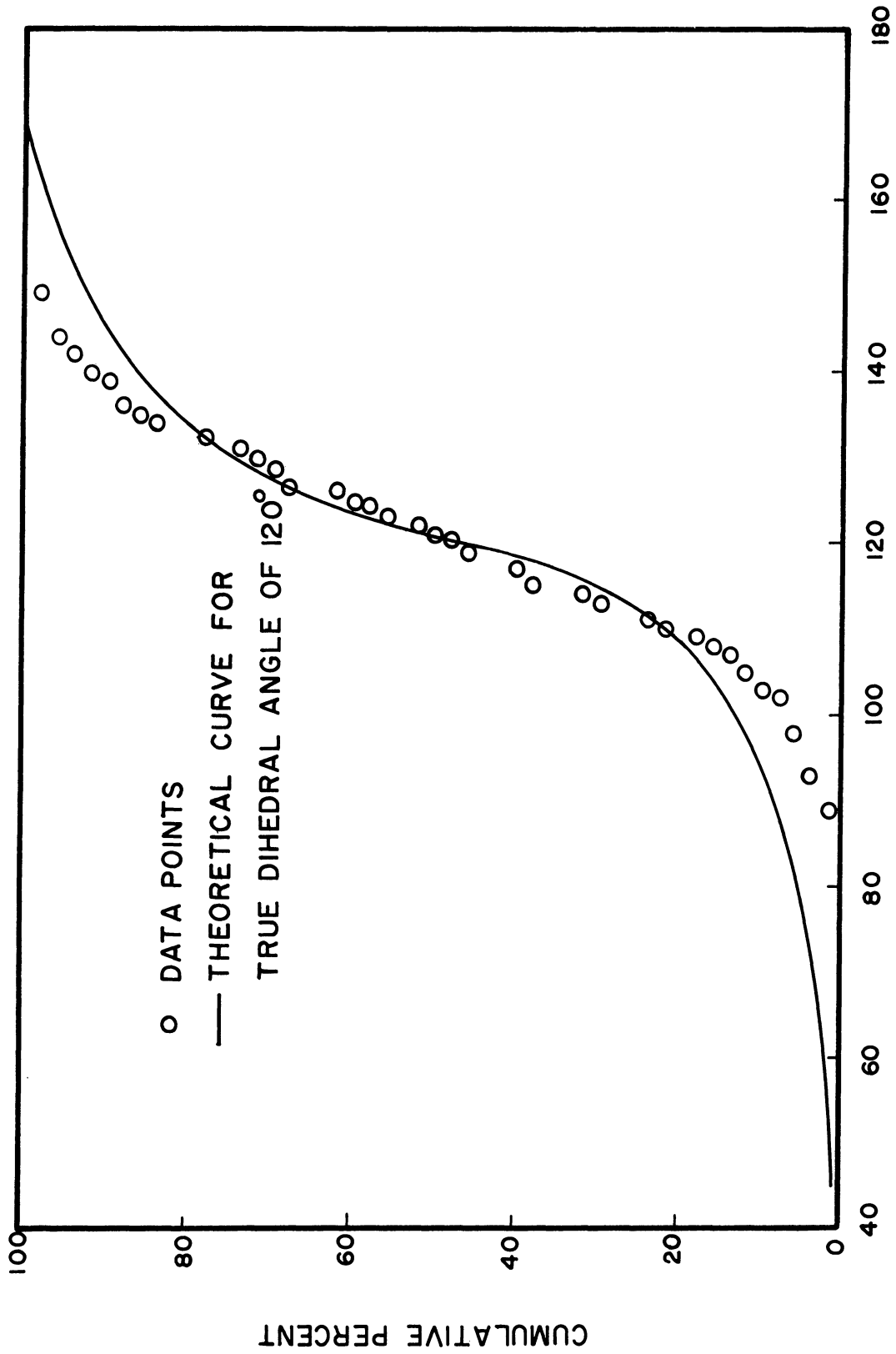

Figure 3. First 50 Data Points on Cross Section of the Molybdenum Sample and the Theoretical Curve for a True Angle of 120°.

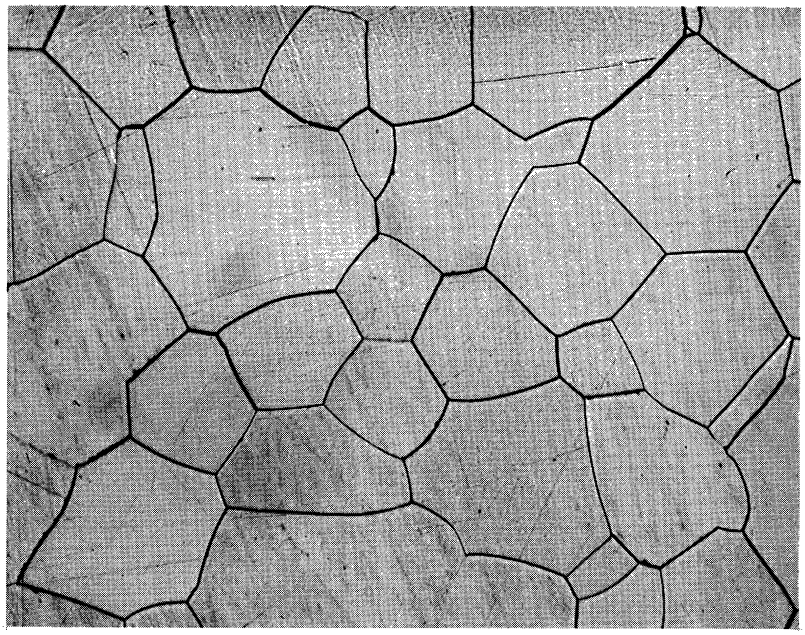

a) Cross Section.

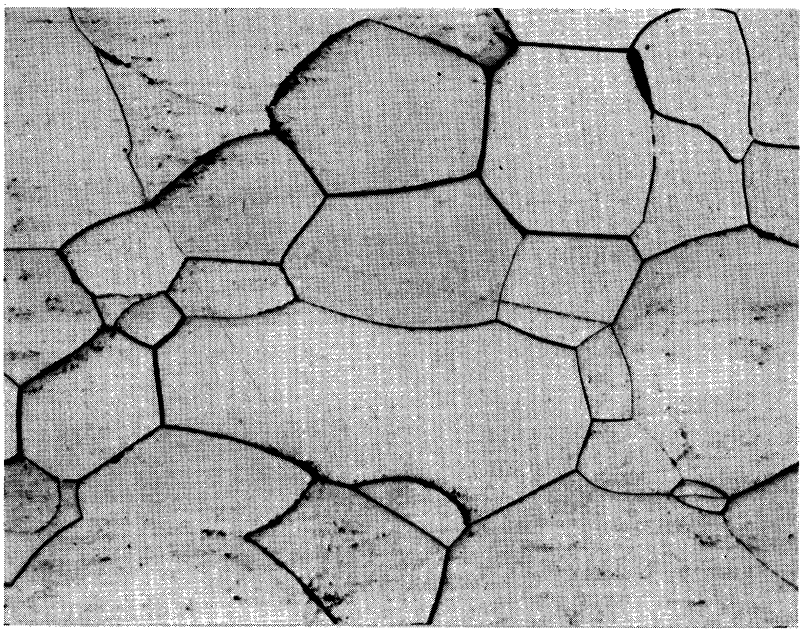

b) Longitudinal Section.

Figure 4. Microstructures of the Molybdenum Sample Etched with 1:1 H_2O_2:NH_4OH. 250X.

B. Silicon-Aluminum Microstructures

The microstructures of silicon-aluminum alloys have been examined after equilibrating at temperatures of 600, 800, and 1000°C. The phase diagram for this system is shown in Figure 5. The alloy composition was adjusted so as to give a primary phase of silicon in an aluminum-rich liquid. A summary of the dihedral angle data is presented in Table IV. The as-solidified microstructure microstructures of samples equilibrated at 600 and 1000°C are shown in Figure 6.

TABLE IV

SUMMARY OF SILICON-ALUMINUM ANGLE DATA

Equilibration Temperature (°C)	Time (Hours)	Number of Angles	True Dihedral Angle (Degrees)	Fit Parameter	Remarks
600	72	100	64	7.30	Random line measuring
800	48	100	55	3.81	"
1000	10	100	40	6.62	"

C. Silicon-Tin Microstructures

The microstructures of silicon-tin alloys were examined after equilibration at temperatures of 600, 800, and 1000°C. The phase diagram for this system is shown in Figure 7. The alloy composition was selected so as to give silicon as the primary phase and a tin rich liquid. A summary of the experimental angle data is presented in Table V.

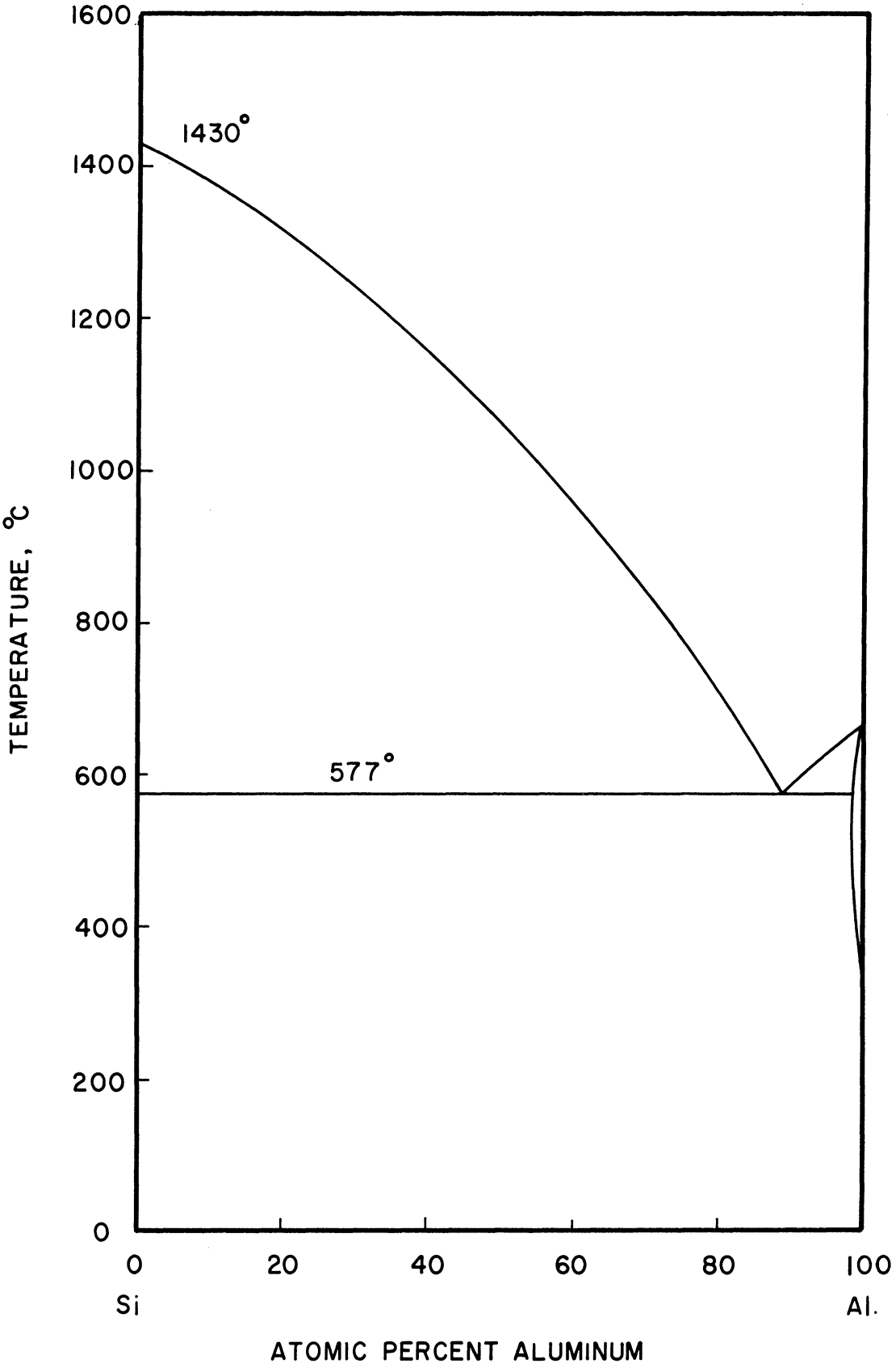

Figure 5. Silicon-Aluminum System (After Hansen[35] and Roberts[36].

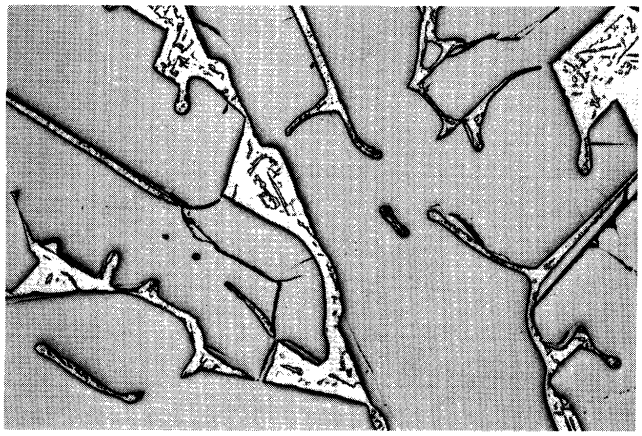

a) As-solidified.

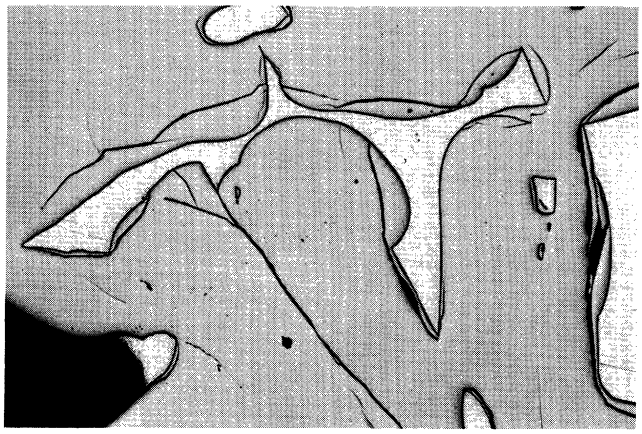

b) Equilibrated at 600°C for 72 hours. True dihedral angle: 64°.

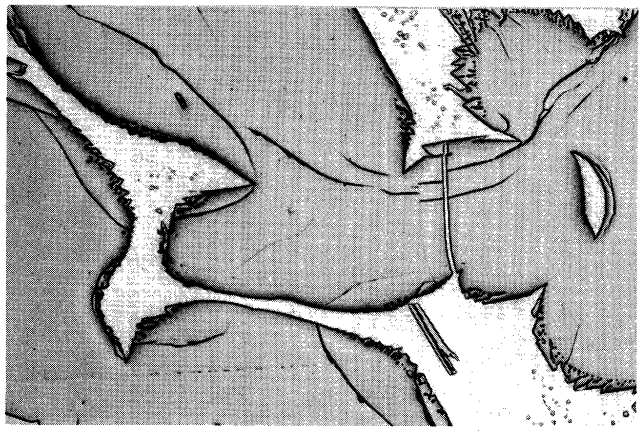

c) Equilibrated at 1000°C for 10 hours. True dihedral angle: 40°.

Figure 6. Microstructures of Silicon-Aluminum Alloys. Unetched. 100X.

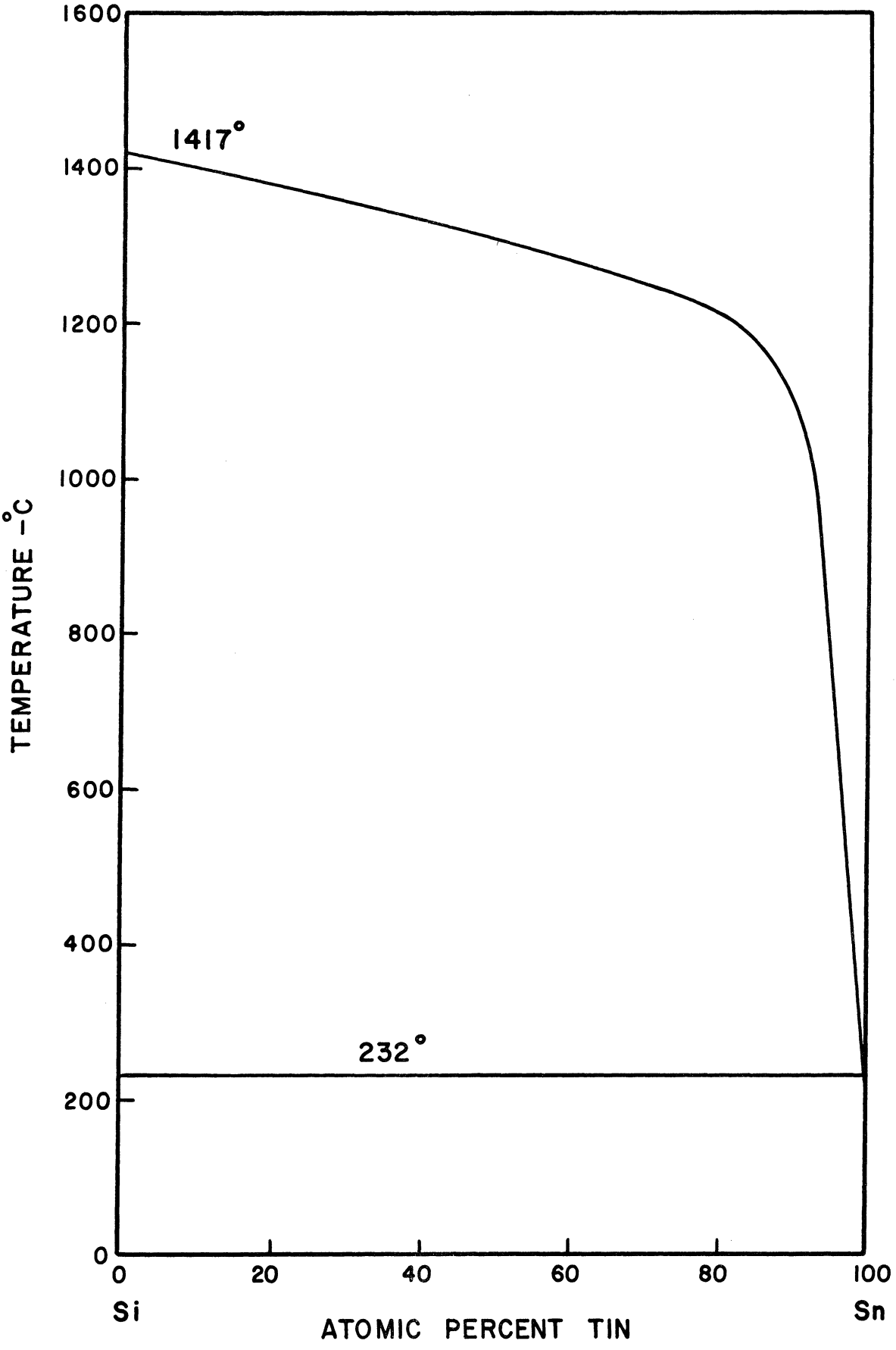

Figure 7. Silicon-Tin System (After Hansen[35] and Tamaru[37]).

TABLE V

SUMMARY OF SILICON-TIN ANGLE DATA

Equilibration Temperature (°C)	Time (Hours)	Number of Angles	True Dihedral Angle (Degrees)	Fit Parameter	Remarks
600	65	50	55	9.59	Very few meaurable angles on sample
600	168	100	63	8.19	Random line measuring
800	48	100	71	5.47	"
1000	24	100	71	4.34	"

The as-solidified microstructure and the microstructure of the sample equilibrated at 1000°C is shown in Figure 8.

D. Nickel-Bismuth Microstructures

The microstructures of nickel-bismuth alloys were examined after they had been equilibrated at temperatures of 700, 900, and 1000°C. The phase diagram for this system is shown in Figure 9. The composition of the alloy was selected so as to give a primary phase of nickel and a liquid phase rich in bismuth. A summary of the dihedral angle data is presented in Table VI. The as-solidified microstructure and microstructures of samples equilibrated at 700 and 900°C are shown in Figure 10.

TABLE VI

SUMMARY OF NICKEL-BISMUTH ANGLE DATA

Equilibration Temperature °C	Time (Hours)	Number of Angles	True Dihedral Angle (Degrees)	Fit Parameter	Remarks
700	74	50	41	4.12	Measured on edge of sample
900	12	50	28	3.67	"
1000	2	100	27	5.05	"

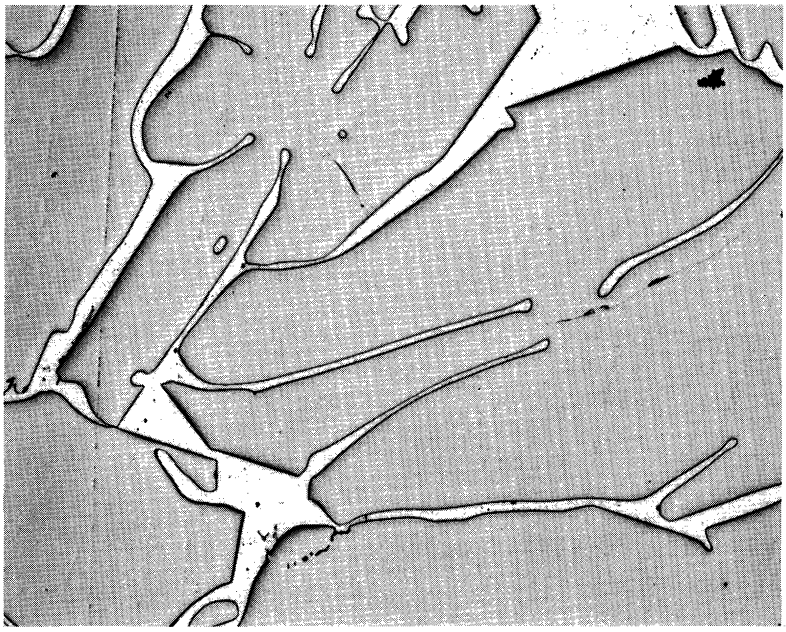

a) As-solidified.

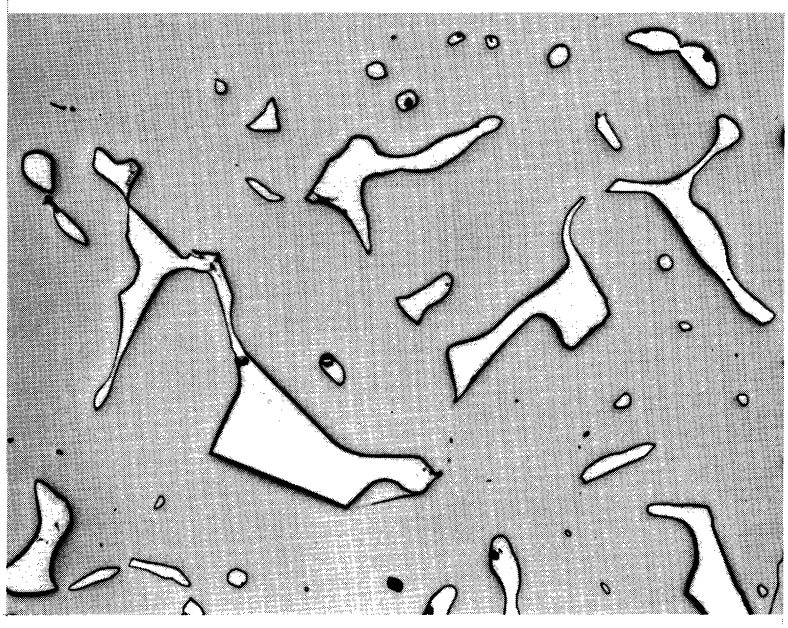

b) Equilibrated at 1000°C for 24 hours. True dihedral angle: 71°.

Figure 8. Microstructures of Silicon-Tin Alloys, Unetched. 100X.

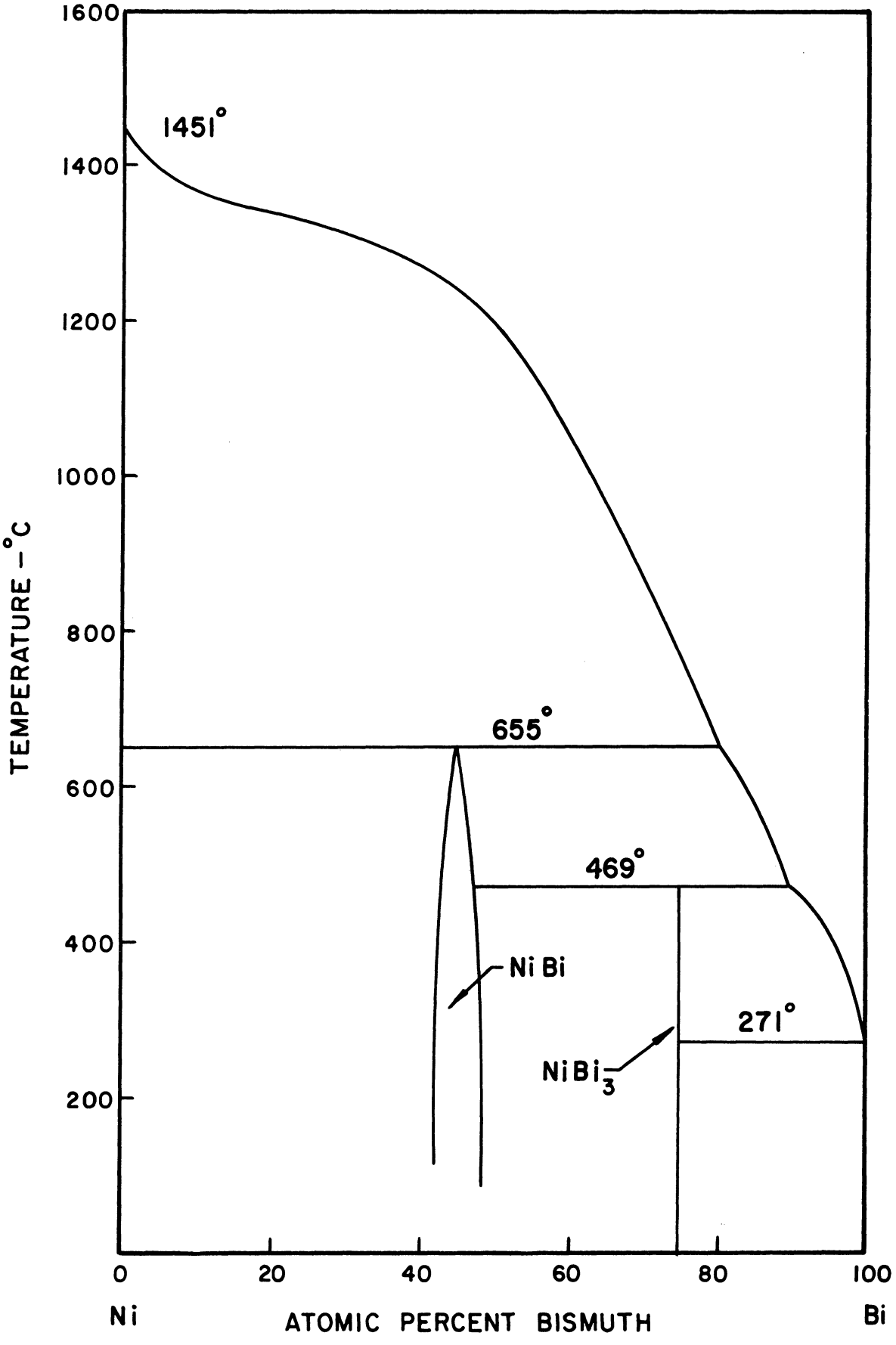

Figure 9. Nickel-Bismuth System (After Hansen[35] and Voss[38]).

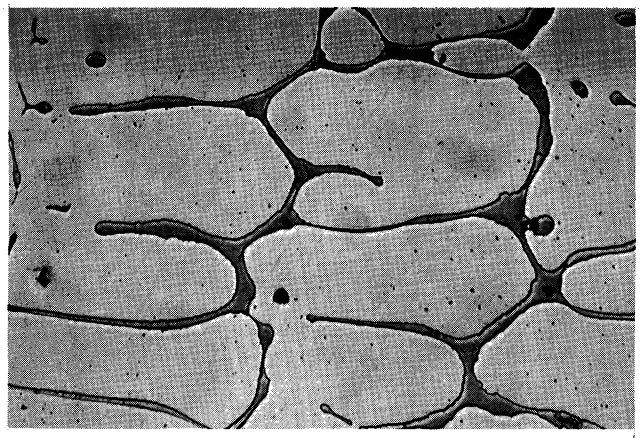

a) As-solidified.

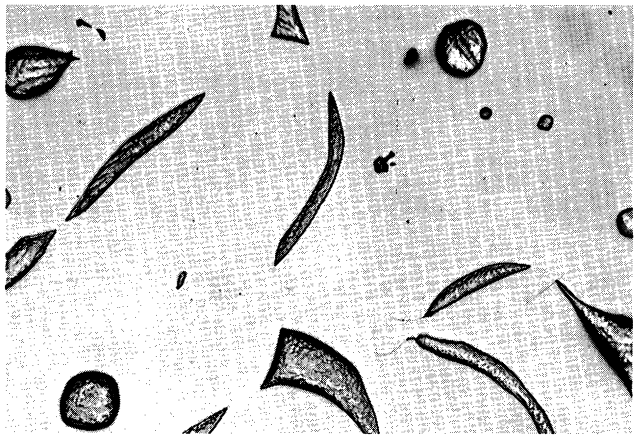

b) Equilibrated at 700°C for 74 hours. True dihedral angle: 41°.

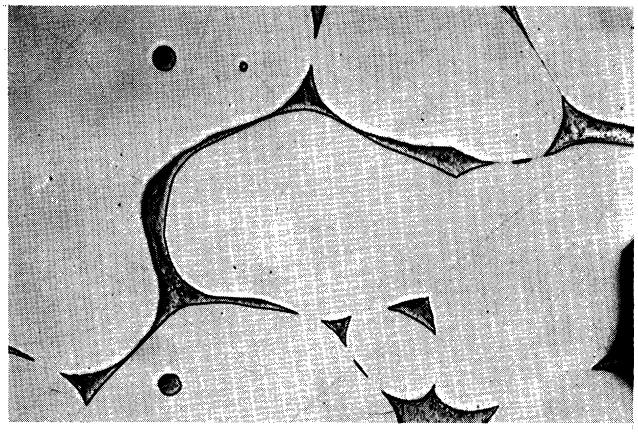

c) Equilibrated at 900°C for 12 hours. True dihedral angle: 28°.

Figure 10. Microstructures of Nickel-Bismuth Alloys. Unetched. 250X.

E. Aluminum-Antimony Microstructures

Microstructures containing the solid phase AlSb in equilibrium with an aluminum-rich liquid and with an antimony-rich liquid were investigated at several temperatures. The phase diagram is reproduced in Figure 11. Several compositions, which had the effect of varying the amount of liquid, were examined on each side of the compound in an effort to determine the effect of the amount of liquid. The data from these experiments are shown in Appendix A. Since there was no detectable effect, the summary of data presented in Table VII has grouped all the angle measurements at a given temperature and on the same side of the compound into one datum point. Aluminum-rich as-solidified and equilibrated microstructures are shown in Figure 12. Antimony-rich as-solidified and equilibrated microstructures of aluminum-antimony alloys are shown in Figure 13.

F. Tin-Tellurium Microstructures

Microstructures containing the solid SnTe phase in equilibrium with a tin-rich liquid and a tellurium-rich liquid were examined after equilibration at various temperatures. The phase diagram for this system is reproduced in Figure 14. Several compositions, containing varying amounts of liquid were studied on each side of the compound. Since there was no consistent variation in microstructure with the amount of liquid, a summary of the data, grouping all measurements made on samples equilibrated at the same temperature and on the same side of the compound is presented in Table VIII. Microstructures of the as-solidified and equilibrated samples on the tin-rich side of the compound are shown in Figure 15. Similar microstructures for tellurium-rich compositions are shown in Figure 16.

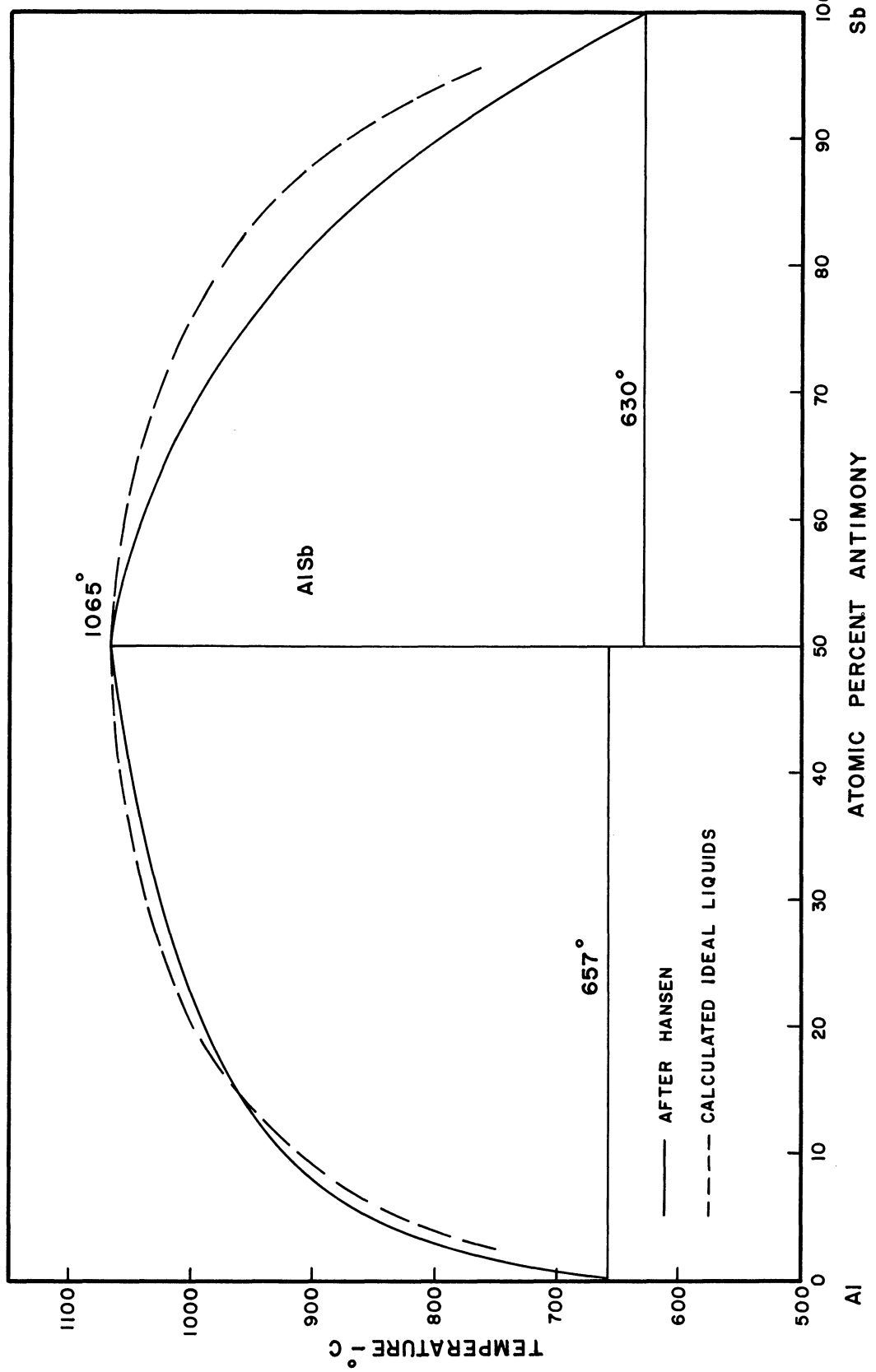

Figure 11. Aluminum-Antimony System (After Hansen[35] and Guertler and Bergmann[39]).

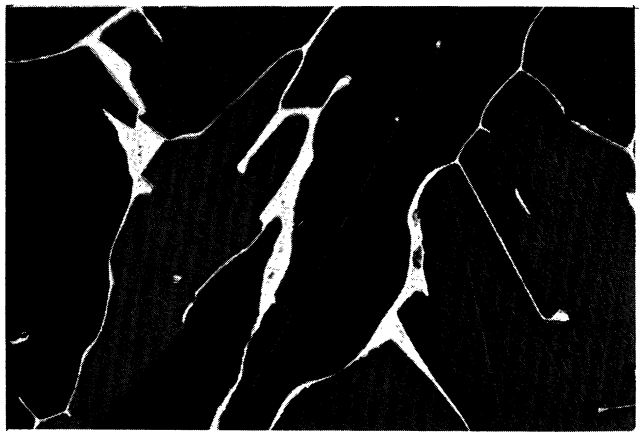

a) As-solidified. 100X.

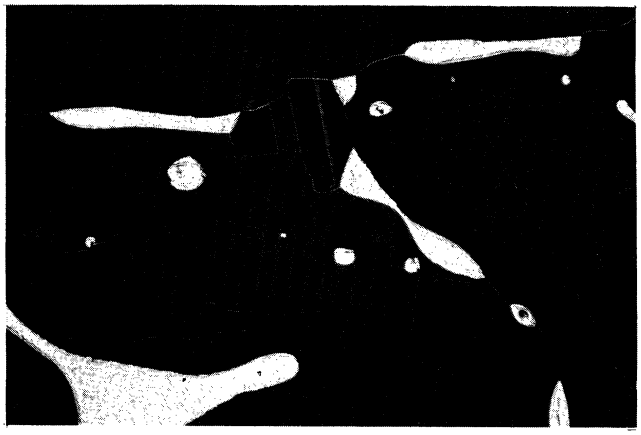

b) Equilibrated at 700°C for 100 hours. True dihedral angle: 78°. 100X.

c) Equilibrated at 950°C for 58 hours. True dihedral angle: 39°. 250X.

Figure 12. Microstructures of Al-rich Aluminum-Antimony Alloys. Unetched.

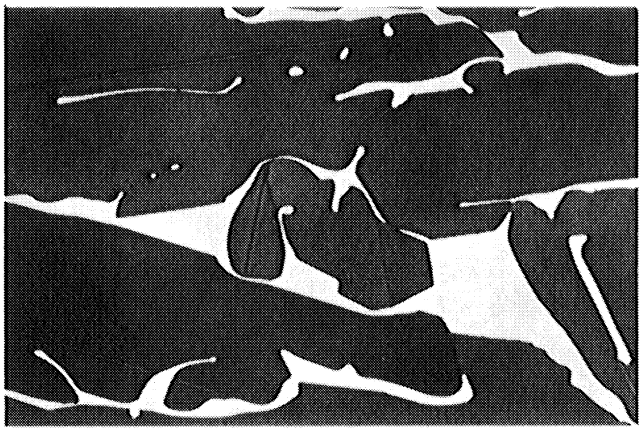

a) As-solidified. 100X.

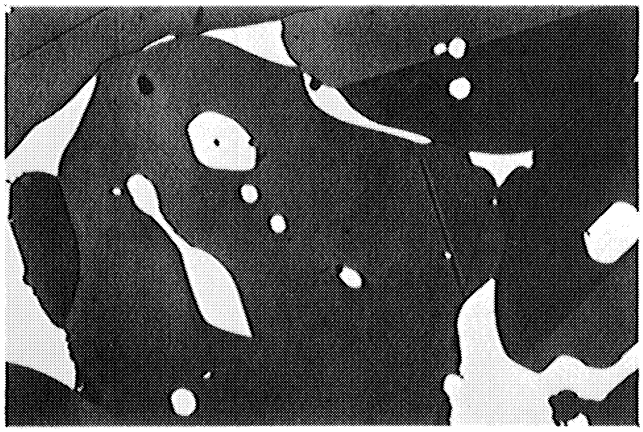

b) Equilibrated at 700°C for 100 hours. True dihedral angle: 56°. 100X.

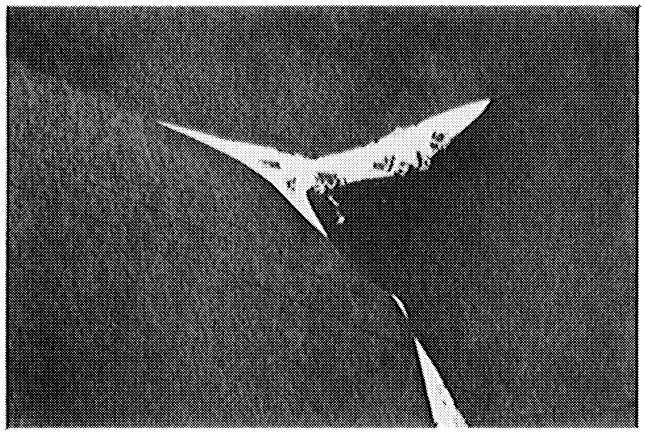

c) Equilibrated at 950°C for 24 hours. True dihedral angle: 31°. 250X.

Figure 13. Microstructures of Sb-rich Aluminum-Antimony Alloys. Unetched.

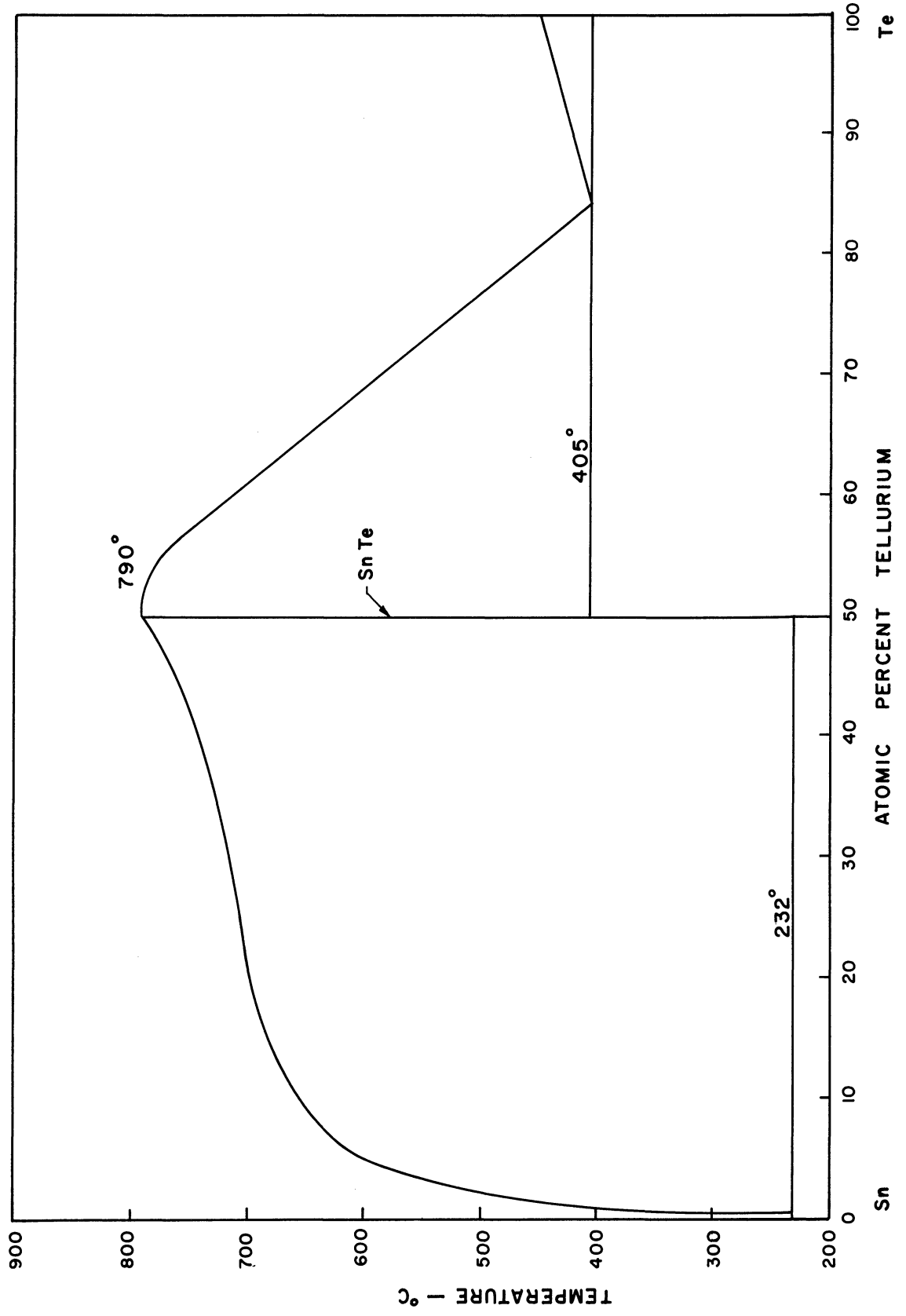

Figure 14. Tin-Tellurium System (After Hansen(35) and Kobayashi(40)).

TABLE VII

SUMMARY OF ALUMINUM-ANTIMONY ANGLE DATA

Equilibration Temperature °C	Number of Specimens	Time (Hours)	Number of Angles	True Dihedral Angle (Degrees)	Fit Parameter
Structures Equilibrated with Aluminum Rich Liquids					
700	2	100	100	78	5.18
800	2	72	100	74	2.79
900	2	48	100	59	2.60
950	2	24-58	100	39	4.59
1000	1	24	50	25	5.07
Structures Equilibrated with Antimony Rich Liquids					
700	4	100	200	56	4.82
800	3	72	150	48	3.00
900	3	48	150	38	3.63
950	3	4-24-46	125	31	4.76
1000	1	26	50	27	6.95

G. Magnesium-Antimony Microstructures

Microstructures containing the solid phase Mg_3Sb_2 were examined after they had been equilibrated at temperatures of 600 and 700°C in the presence of an antimony-rich liquid. The phase diagram for this system is reproduced in Figure 17. Compositions were selected so as to give the Mg_3Sb_2 as the primary solid phase and a liquid rich in antimony. A summary of the experimental dihedral angle data is presented in Table IX.

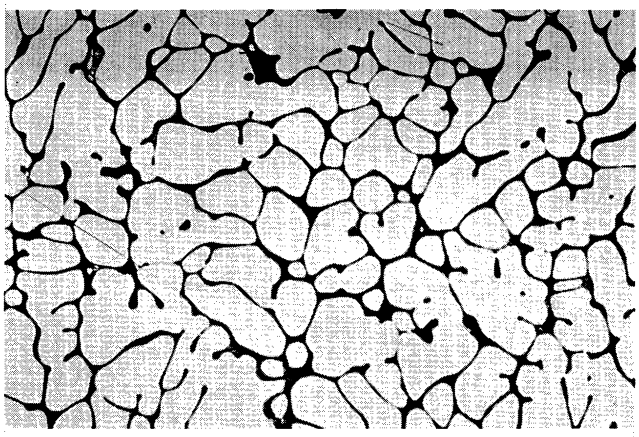

a) As-solidified.

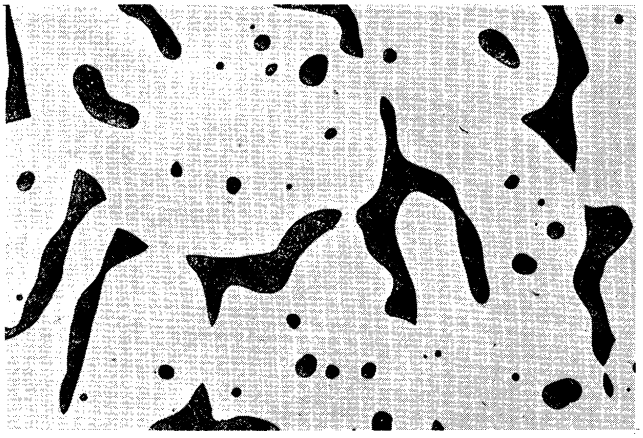

b) Equilibrated at 300°C for 138 hours. True dihedral angle: 77°.

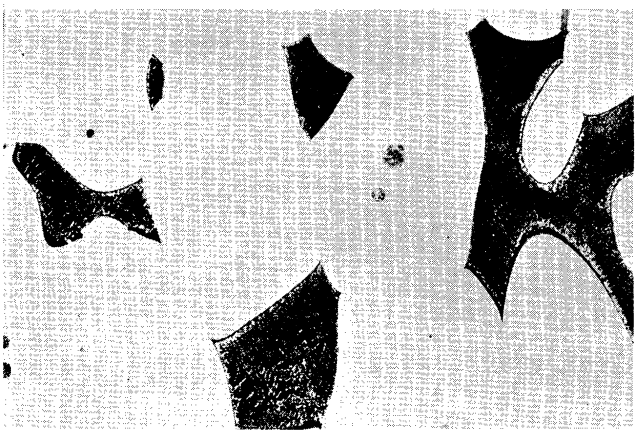

c) Equilibrated at 700°C for 24 hours. True dihedral angle: 46°.

Figure 15. Microstructures of Sn-rich Tin-Tellurium Alloys. Etched with 2% Nital. 100X.

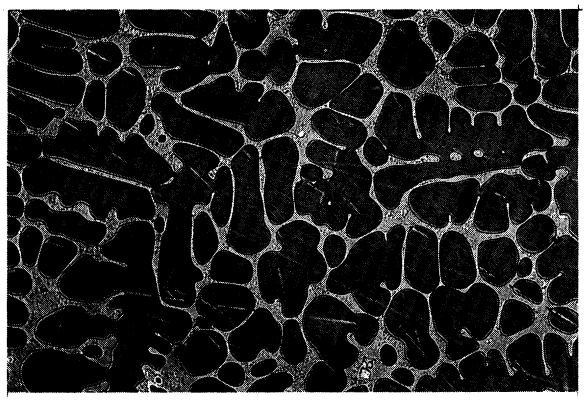

a) As-solidified.

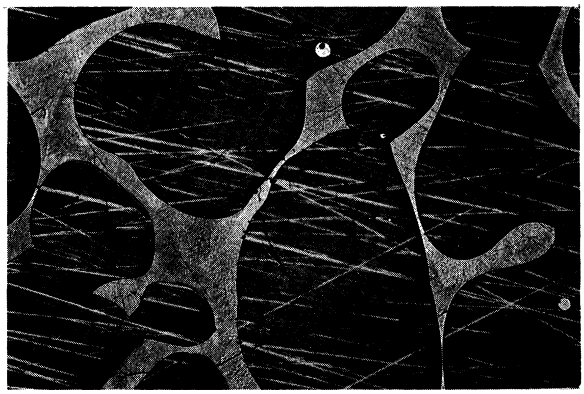

b) Equilibrated at 450°C for 72 hours.
True dihedral angle: 58°.

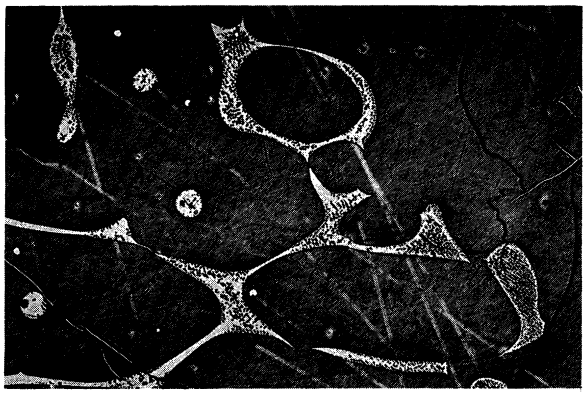

c) Equilibrated at 600°C for 4 hours.
True dihedral angle: 39°.

Figure 16. Microstructures of Te-Rich Tin-Tellurium Alloys. Etched with D-4 Etchant.* 100X.

*D-4 Etchant

45 gr $CuCl_2$/300 ml H_2O	290 ml
Acetic acid	330 ml
Concentrated HCl	230 ml
CrO_3 33 gr/100 ml H_2O	70 ml
Concentrated HNO_3	30 ml
Concentrated H_2SO_4	50 ml
Concentrated HF	25 ml

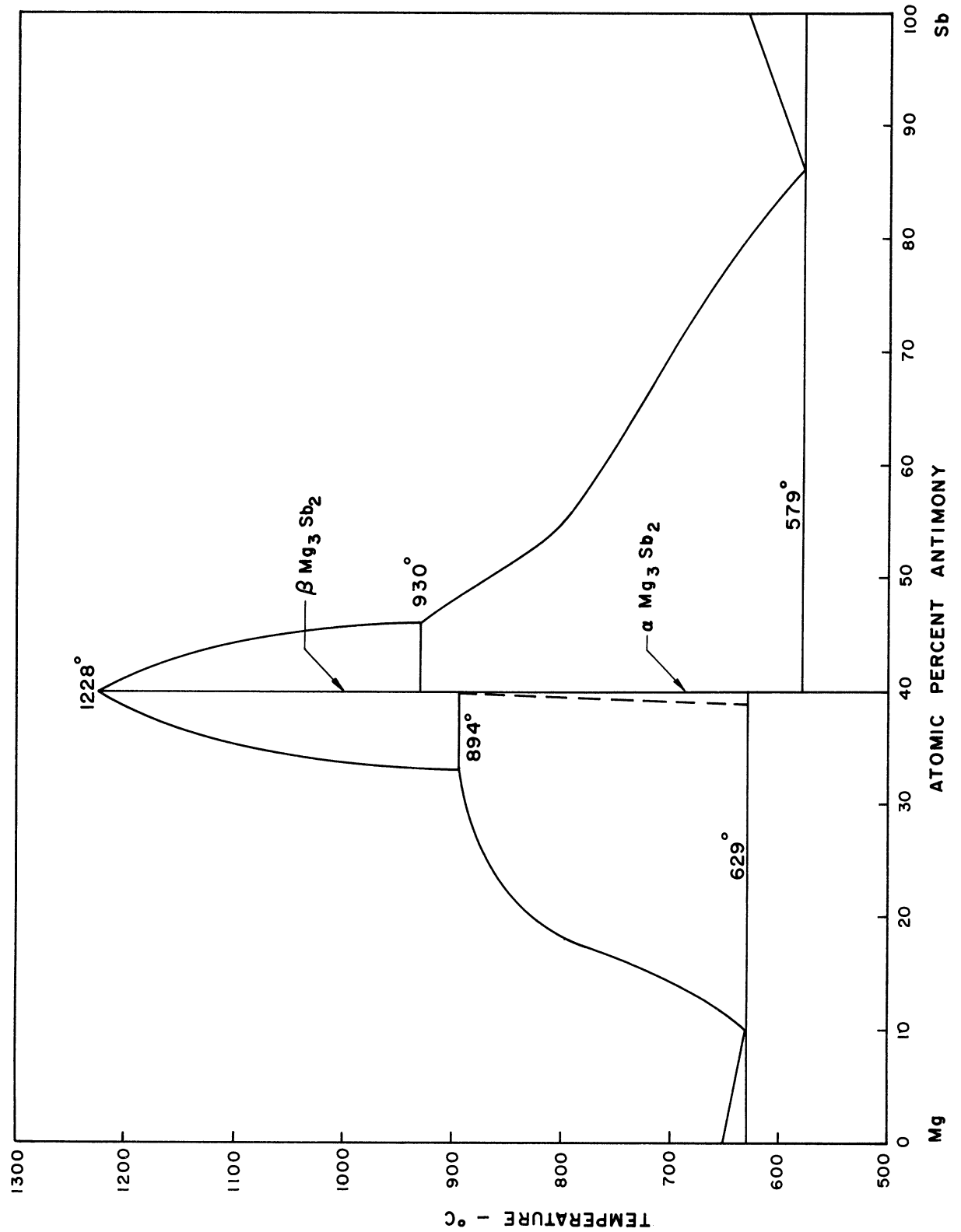

Figure 17. Magnesium-Antimony System (After Hansen[35] and Grube and Barnhok[41]).

TABLE VIII

SUMMARY OF TIN-TELLURIUM ANGLE DATA

Equilibration Temperature °C	Number of Specimens	Time (Hours)	Number of Angles	True Dihedral Angle (Degrees)	Fit Parameter
Structures Equilibrated with Aluminum-Rich Liquids					
300	3	138	350	77	6.74
450	2	48	150	79	4.60
500	5	48-72-96	125	74	4.34
550	2	48	150	77	4.75
600	5	2-4-12-24	225	63	6.21
650	2	20	150	61	3.79
700	2	24	150	46	5.28
Structures Equilibrated with Tellurium-Rich Liquids					
450	3	26-72	125	58	8.21
500	8	4-6-16-24-48-72-96	350	47	8.42
550	2	6-16	100	45	6.74
600	3	4-6-16	175	39	7.17

TABLE IX

SUMMARY OF MAGNESIUM-ANTIMONY ANGLE DATA

Equilibration Temperature °C	Time (Hours)	Number of Angles	True Dihedral Angle (Degrees)	Fit Parameter
600	20	100	54	5.59
700	24	100	33	2.33

The as-solidified microstructure and photomicrographs of the microstructures equilibrated at 600 and 700°C are shown in Figure 18.

H. Aluminum-Indium-Antimony Microstructures

Microstructures containing the solid AlSb in equilibrium with an aluminum-indium-rich liquid were examined after equilibration at 800°C. The ternary phase diagram for this system is reproduced in Figure 19. Microstructures composed of the solid AlSb and an indium-antimony-rich liquid were examined after equilibration at 700 and 800°C. A summary of the experimental dihedral angle data is presented in Table X.

TABLE X

SUMMARY OF ALUMINUM-INDIUM-ANTIMONY ANGLE DATA

Equilibration Temperature °C	Composition	Number of Samples	Time (Hours)	Number of Angles	True Dihedral Angle (Degrees)	Fit Parameter
700	In-Sb-rich	2	72-120	100	57	3.52
800	In-Sb-rich	1	72	50	48	4.89
800	Al-In-rich	2	72	100	67	3.59

Photomicrographs of the two microstructures equilibrated at 800°C are shown in Figure 20.

I. Periclase (MgO) Microstructures

Microstructures containing the solid phase periclase (MgO) were examined after they had been equilibrated at various temperatures as dictated by the known phase relationships, with the following oxide liquids, all of which are saturated with MgO.

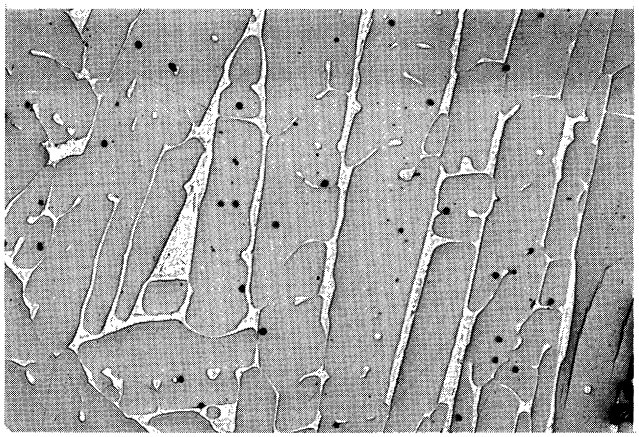

a) As-solidified.

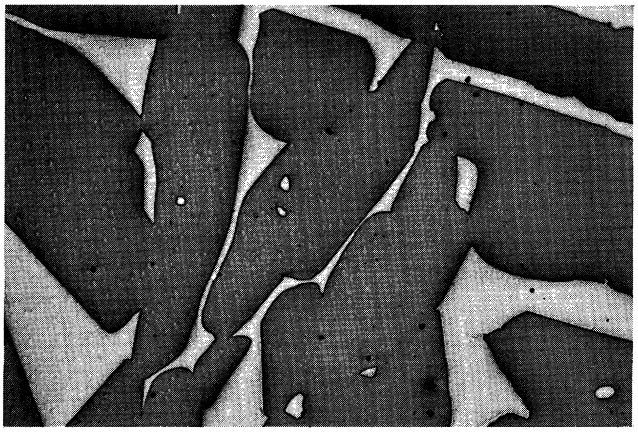

b) Equilibrated at 600°C for 20 hours. True dihedral angle: 54°.

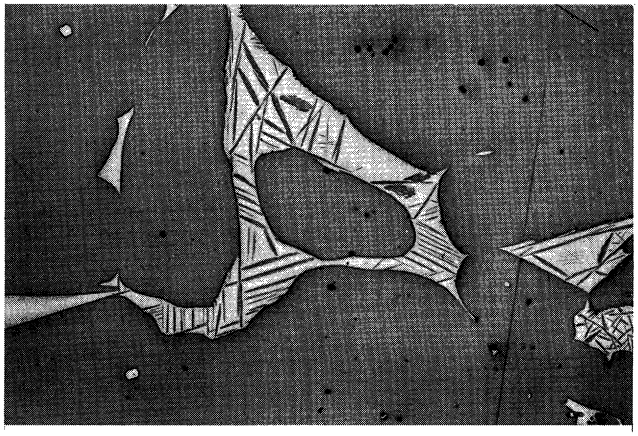

c) Equilibrated at 700°C for 24 hours. True dihedral angle: 33°.

Figure 18. Microstructures of Sb-rich Magnesium-Antimony Alloys. Unetched. 100X.

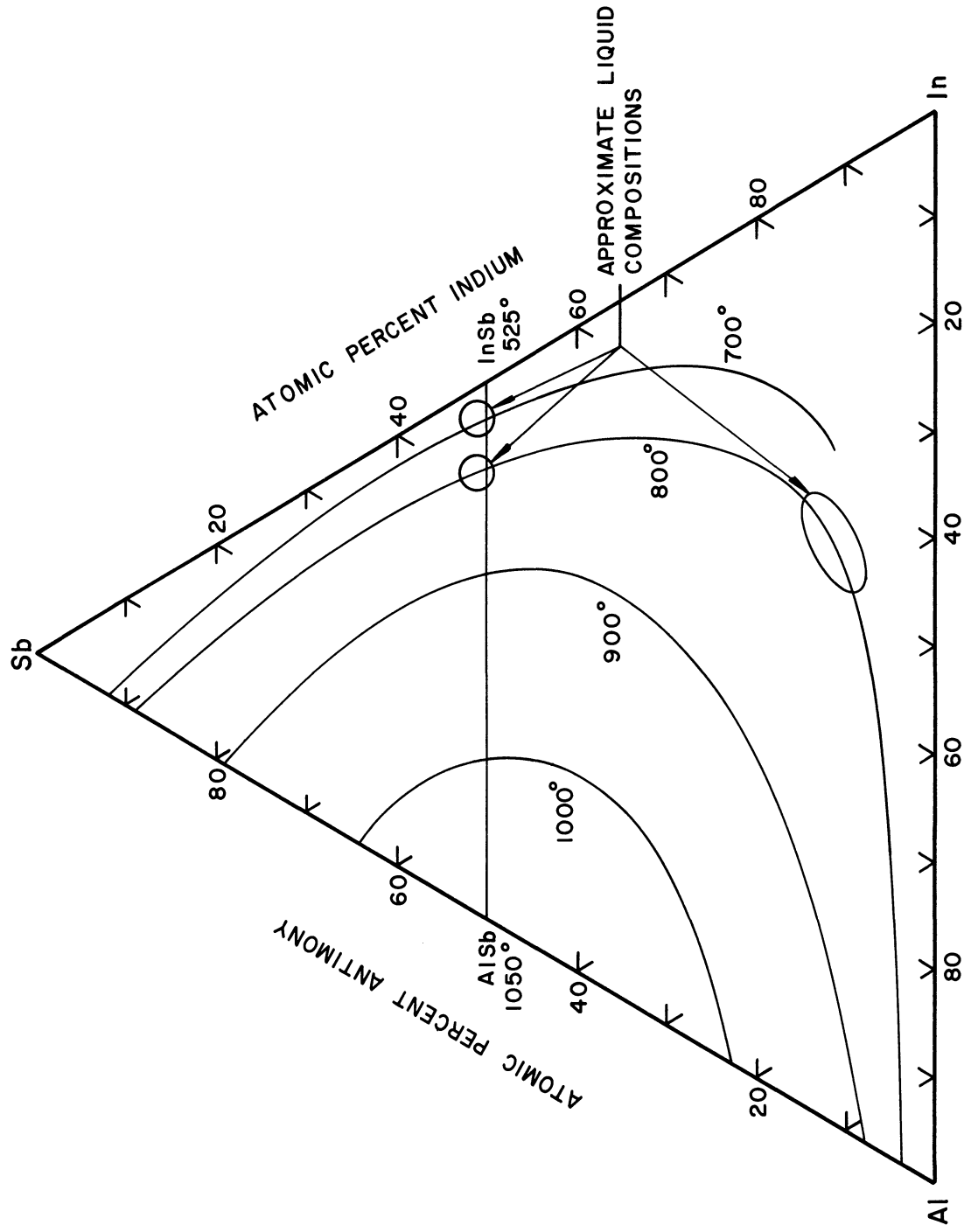

Figure 19. Aluminum-Indium-Antimony System (After Koster and Thoma[42]).

a) Aluminum-indium-rich liquid. True dihedral angle: 67°.

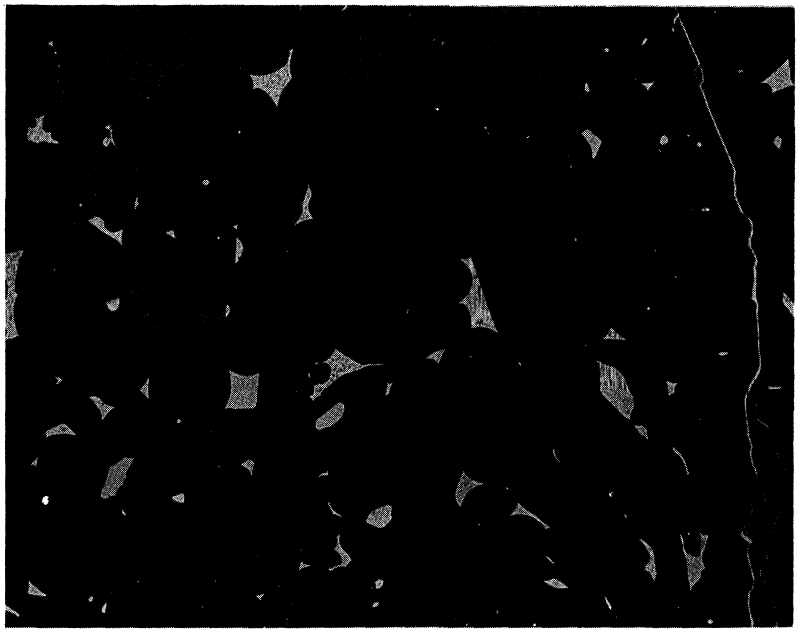

b) Indium-antimony-rich liquid. True dihedral angle: 48°.

Figure 20. Equilibrated Microstructures Containing the Solid Phase AlSb and Various Liquids as Quenched from 800°C After 72 hours. Unetched. 100X.

1. SiO_2-rich SiO_2-CaO liquid
2. CaO-rich SiO_2-CaO liquid
3. Al_2O_3-rich Al_2O_3-CaO liquid
4. CaO-rich Al_2O_3-CaO liquid
5. $4CaO \cdot Al_2O_3 \cdot Fe_2O_3$ liquid .

The ternary phase diagram for the system CaO-MgO-SiO_2 is reproduced in Figure 21 on both the weight percent and mole percent bases. Similar diagrams for the system CaO-MgO-Al_2O_3 are reproduced in Figure 22. The pseudo-binary phase diagram for the system $4CaO \cdot Al_2O_3 \cdot Fe_2O_3$-MgO is reproduced in Figure 23. Several compositions which produced only a change in the amount of liquid were run at each condition of temperature and liquid composition. Since there was no detectable change in the geometry with the amount of liquid, within the limits studied, all the dihedral angles measured on samples with the same liquid composition and temperature are grouped into a single datum point. A summary of all such data for structures involving periclase is presented in Table XI.

TABLE XI

SUMMARY OF PERICLASE (MgO) DIHEDRAL ANGLE DATA

Equilibration Temp. °C	Liquid Composition	Number of Samples	Time (hours)	Number of Angles	True Dihedral Angle (Degrees)	Fit Parameter
1500	CaO-rich Al_2O_3-CaO	3	64	150	33	4.48
1500	Al_2O_3-rich Al_2O_3-CaO	3	64	125	31	7.16
1600	SiO_2-rich CaO-SiO_2	2	64	200	22	5.51
1600	CaO-rich CaO-SiO_2	2	64	200	24	6.56
1600	Al_2O_3-rich Al_2O_3-CaO	2	64	200	31	5.06
1600	CaO-rich Al_2O_3-CaO	2	64	125	29	4.16
1600	$4CaO \cdot Al_2O_3 \cdot Fe_2O_3$-rich	3	64	300	30	5.51

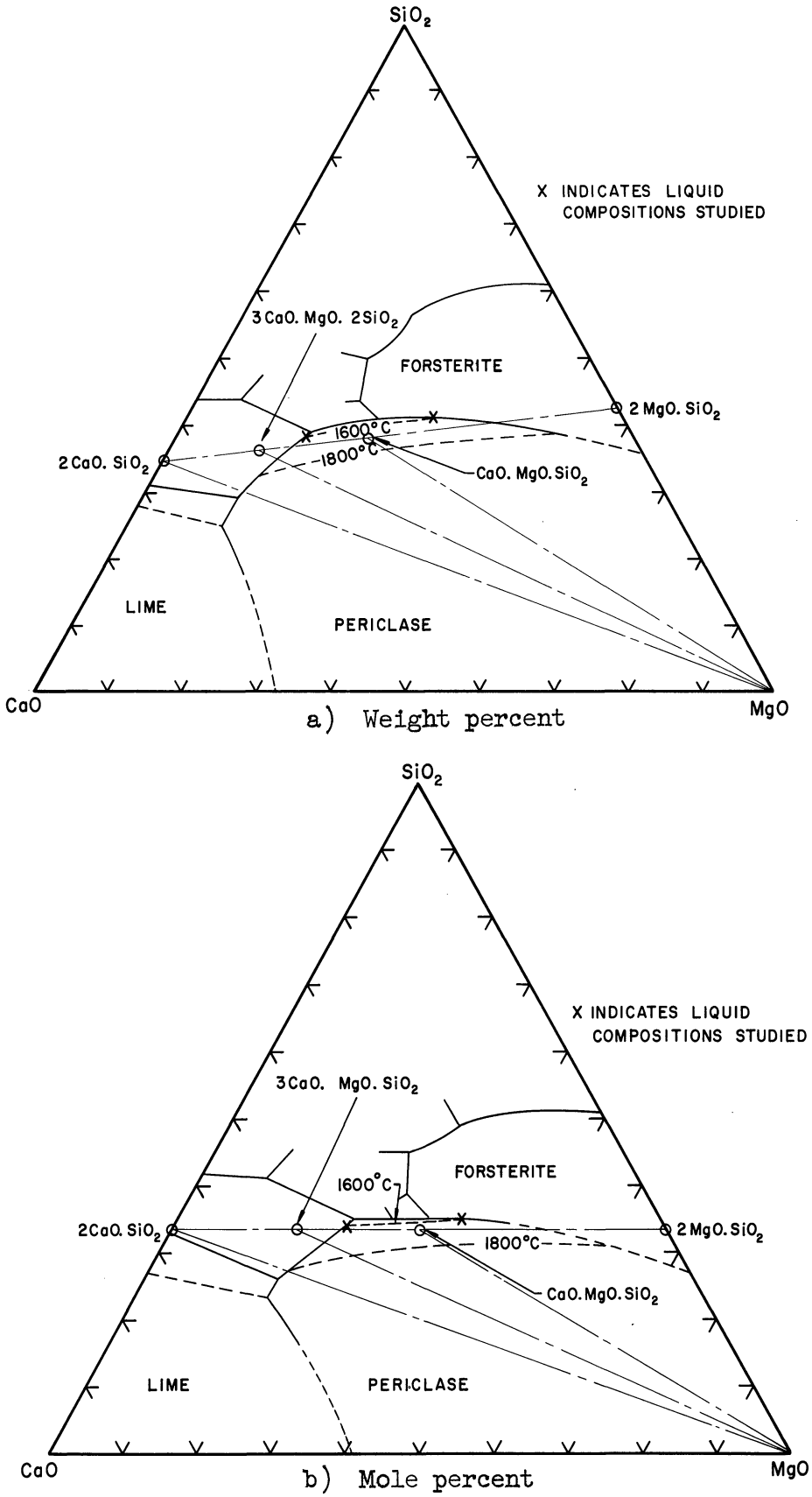

Figure 21. System CaO-MgO-SiO_2. (After Osborn and Muan[43] and Ricker and Osborn[44]).

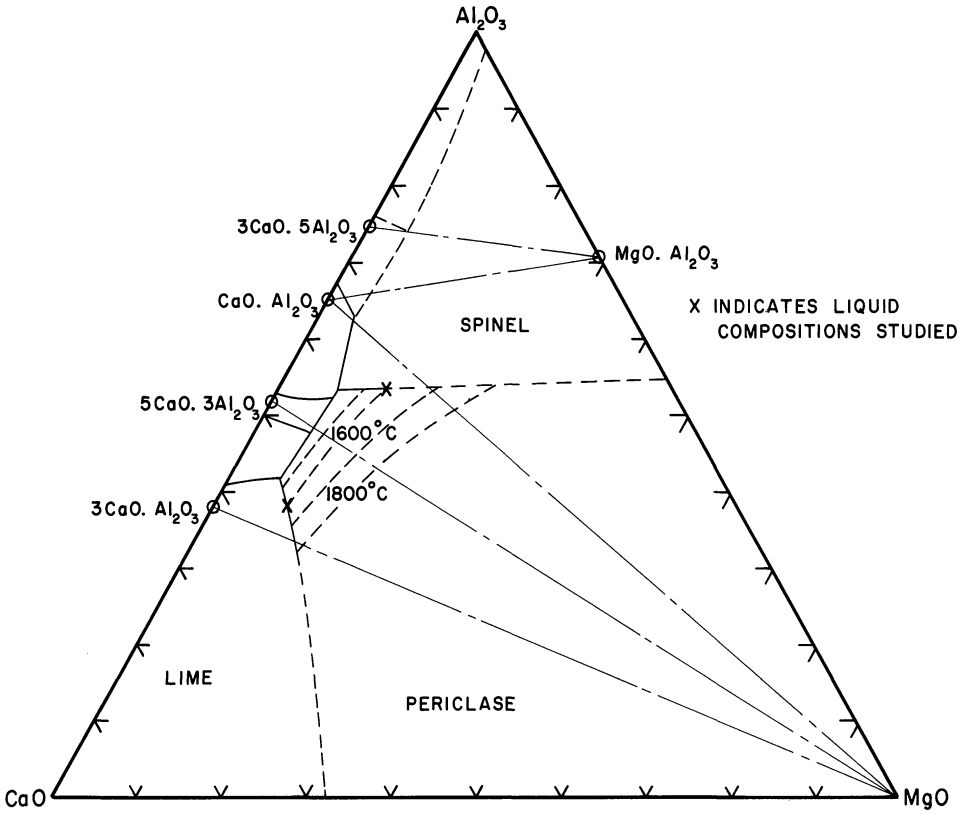

a) Weight percent

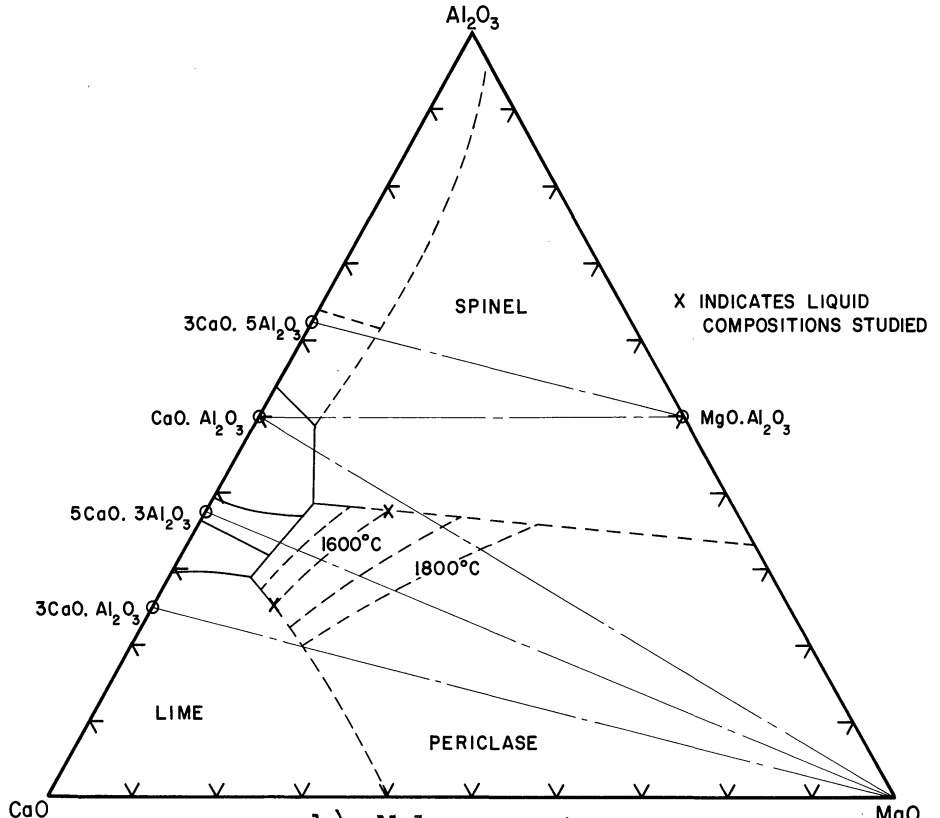

b) Mole percent

Figure 22. System CaO-MgO-Al_2O_3. (After Sosman and Andersen[45] and Rankin and Merwin[46]).

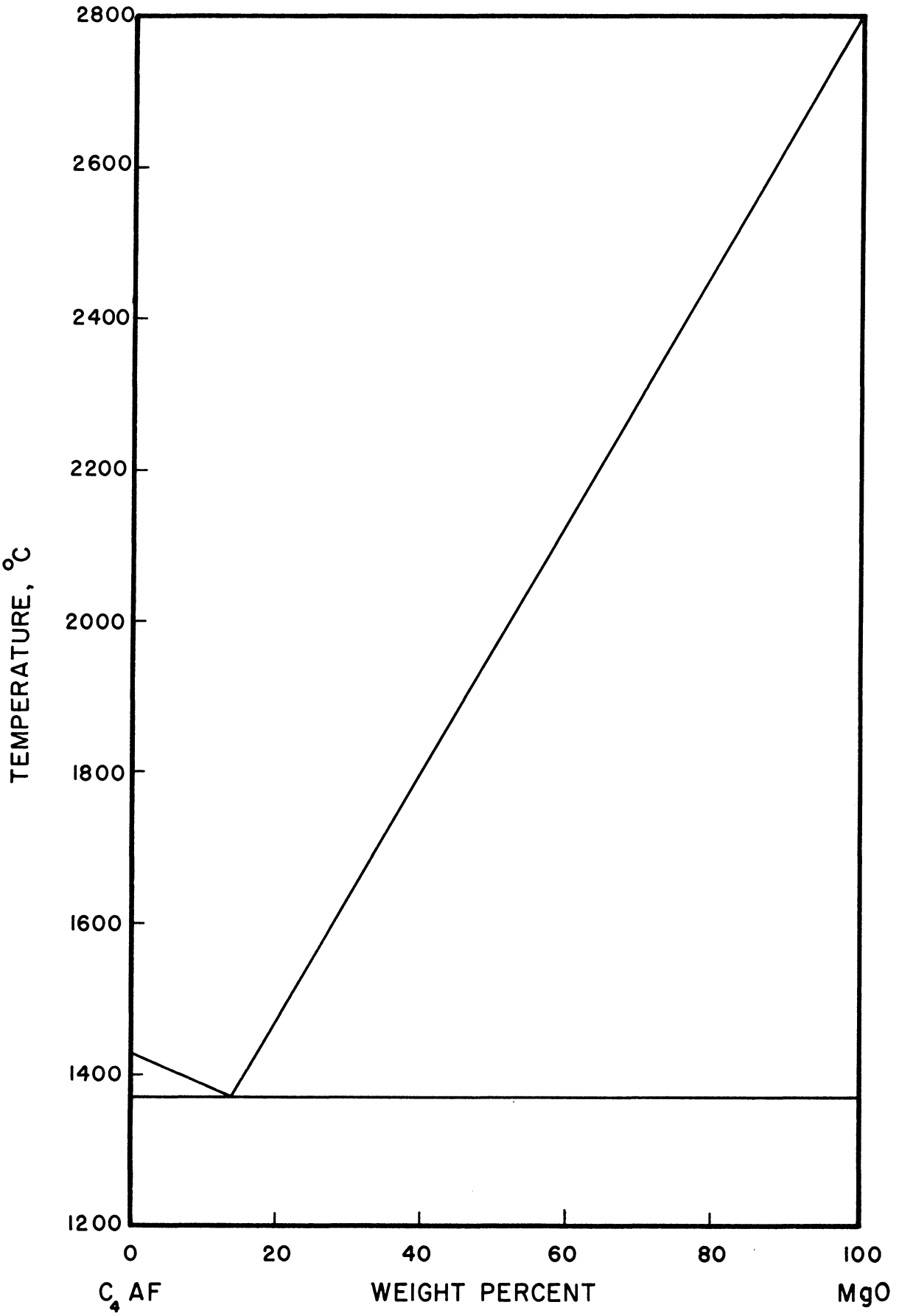

Figure 23. System $4CaO \cdot Al_2O_3 \cdot Fe_2O_3$-MgO; C = CaO, A = Al_2O_3, F = Fe_2O_3. (After Rait[47]).

Photomicrographs of the microstructures found in the SiO_2 ternary are shown in Figure 24, and in the Al_2O_3 ternary are shown in Figure 25. Microstructures found in the pseudo-binary involving $4CaO \cdot Al_2O_3 \cdot Fe_2O_3$ and MgO are shown in Figure 31 in the section covering grain growth.

2. Grain Growth

During the course of this investigation it was noted that there were some striking differences in the mode of growth of the individual crystallites for the different types of materials studied. These differences may be attributed to anisotropic growth rates and the response of microstructures to interfacial tension forces. The influence of time at temperature for a structure involving the solid phase AlSb is shown in the photomicrographs of Figure 26. A similar series of photomicrographs of structures involving the solid phase SnTe are found in Figure 27.

A more extensive study of the effects of time, temperaure, and the composition of the liquid phase on grain growth was conducted in systems involving the solid phase periclase (MgO). Results of the effect of time and liquid composition at constant temperature are summarized in Table XII and typical results are shown graphically in Figure 28. Typical photomicrographs are shown in Figure 29. Results of the effect of increasing temperature at constant time and relatively constant liquid composition on the rate of grain growth are summarized in Table XIII and are shown graphically in Figure 30. Photomicrographs of typical structures are shown in Figure 31.

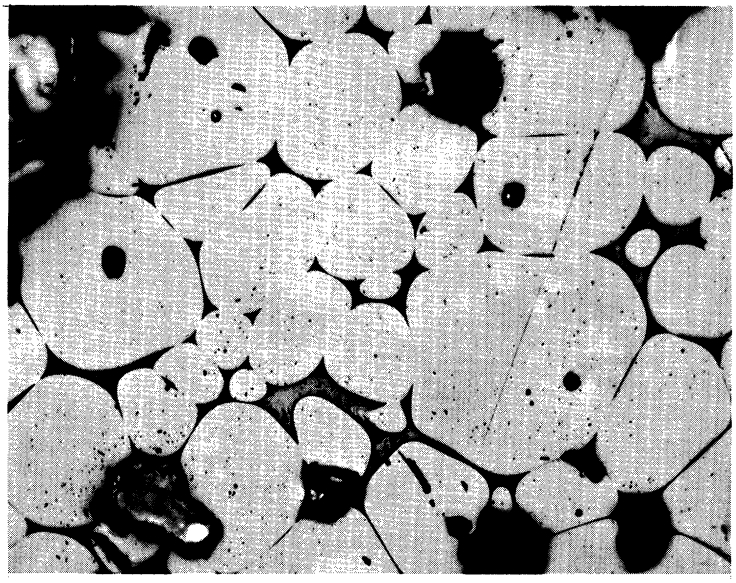

a) SiO_2-rich CaO-SiO_2 liquid. True dihedral angle: 22°.

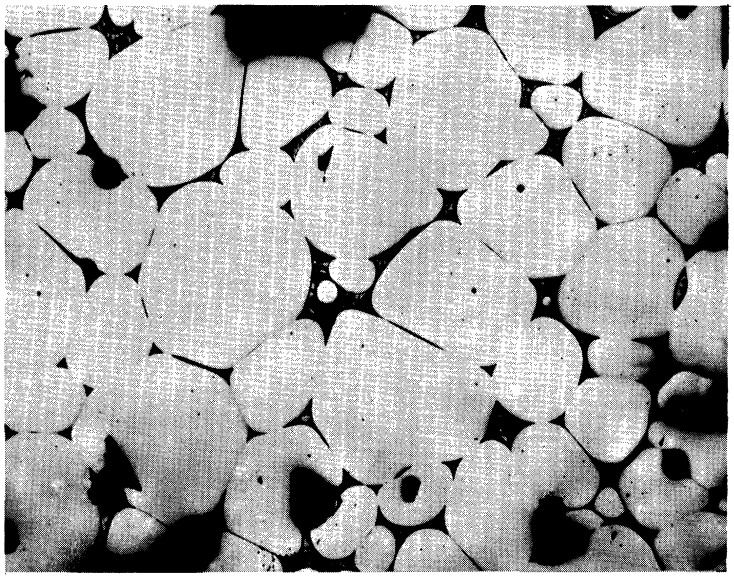

b) CaO-rich CaO-SiO_2 liquid. True dihedral angle: 24°.

Figure 24. Equilibrated Microstructures Containing the Solid Phase Periclase (MgO) and Various Liquids as Quenched from 1600°C After 64 Hours. Etched with 5% HF. 250X.

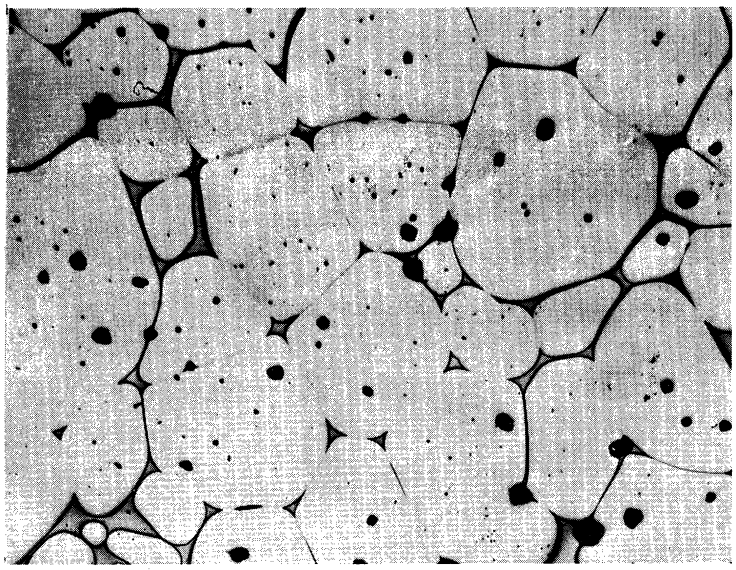

a) Al_2O_3-rich Al_2O_3-CaO liquid. True dihedral angle: 31°.

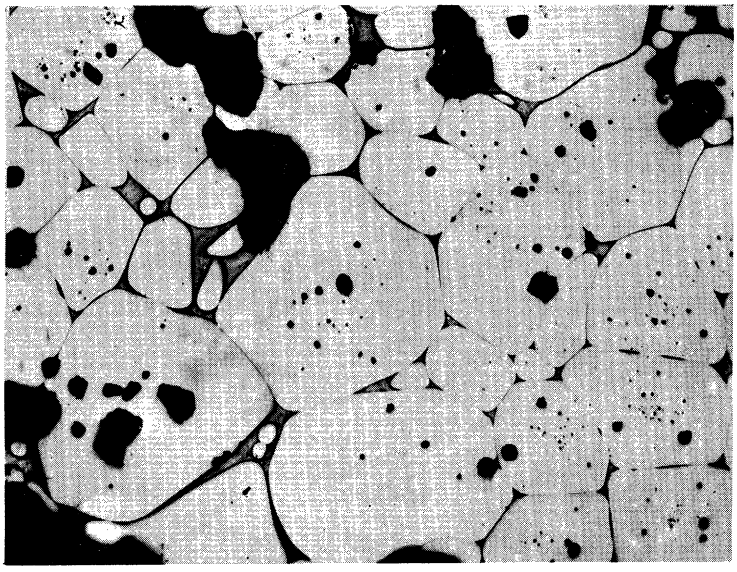

b) CaO-rich Al_2O_3-CaO liquid. True dihedral angle: 29°.

Figure 25. Equilibrated Microstructures Containing the Solid Phase Periclase (MgO) and Various Liquids as Quenched from 1600°C After 64 Hours. Etched with 5% HF. 250X.

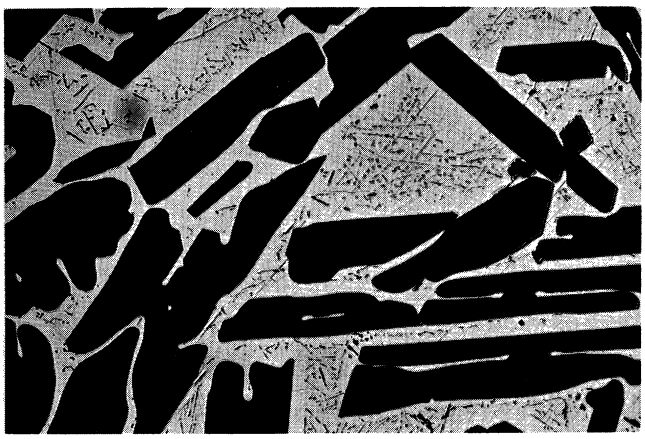

a) As-solidified.

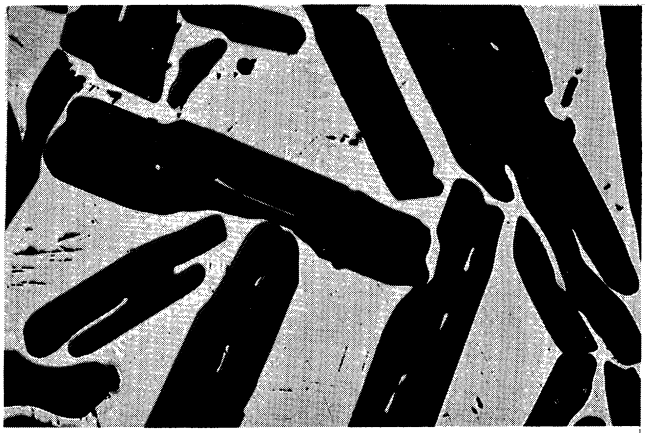

b) 48 hours.

c) 100 hours.

Figure 26. Grain Growth of AlSb with Time in the Presence of a Sb-Rich Liquid at 700°C. Unetched. 100X.

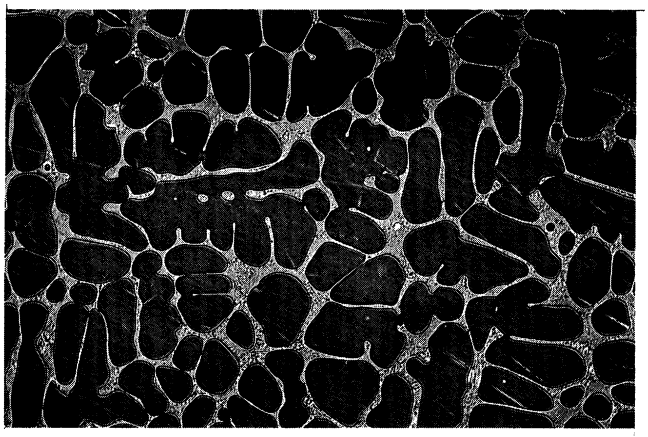

a) As-solidified.

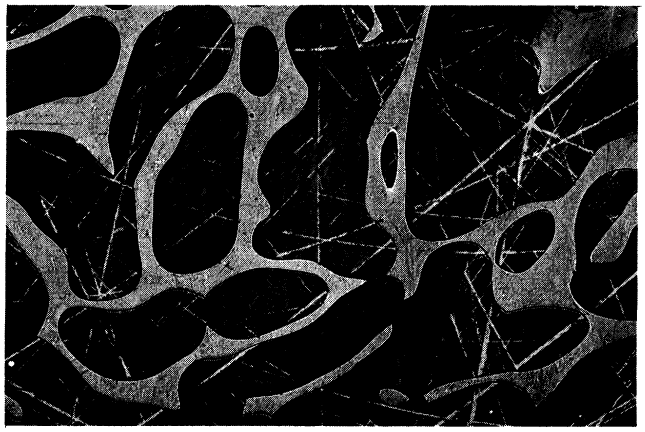

b) 4 hours.

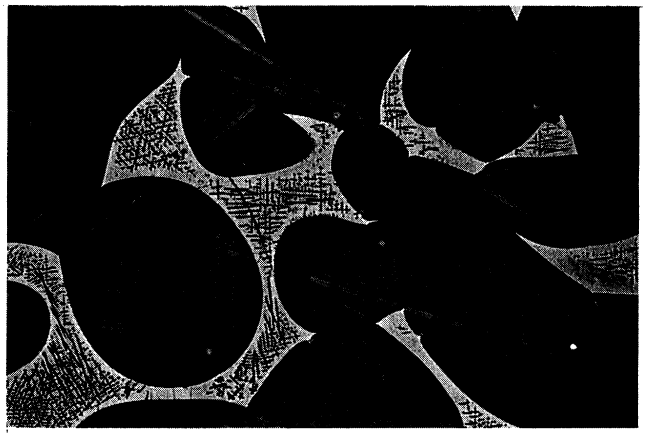

c) 96 hours.

Figure 27. Grain Growth of SnTe with Time in the Presence of a Te-Rich Liquid at 500°C. Etched with D-4. 100X.

TABLE XII

SUMMARY OF PERICLASE (MgO) GRAIN GROWTH DATA AT CONSTANT TEMPERATURE

Temperature °C	Time (Hours)	Liquid Composition	Grain Diameter (mm.)
1400	4	$4CaO \cdot Al_2O_3 \cdot Fe_2O_3$-rich	0.0353
1400	36	"	0.0672
1400	64	"	0.0816
1600	4	CaO-rich $CaO-SiO_2$	0.0282
1600	16	"	0.0383

TABLE XIII

SUMMARY OF PERICLASE (MgO) GRAIN GROWTH DATA VS TEMPERATURE

Temperature °C	Time (Hours)	Liquid Composition	Grain Diameter (mm.)
1400	4	$4CaO \cdot Al_2O_3 \cdot Fe_2O_3$-rich	0.0288
1600	4	"	0.0459
1700	4	"	0.0724
1800	4	"	0.0879

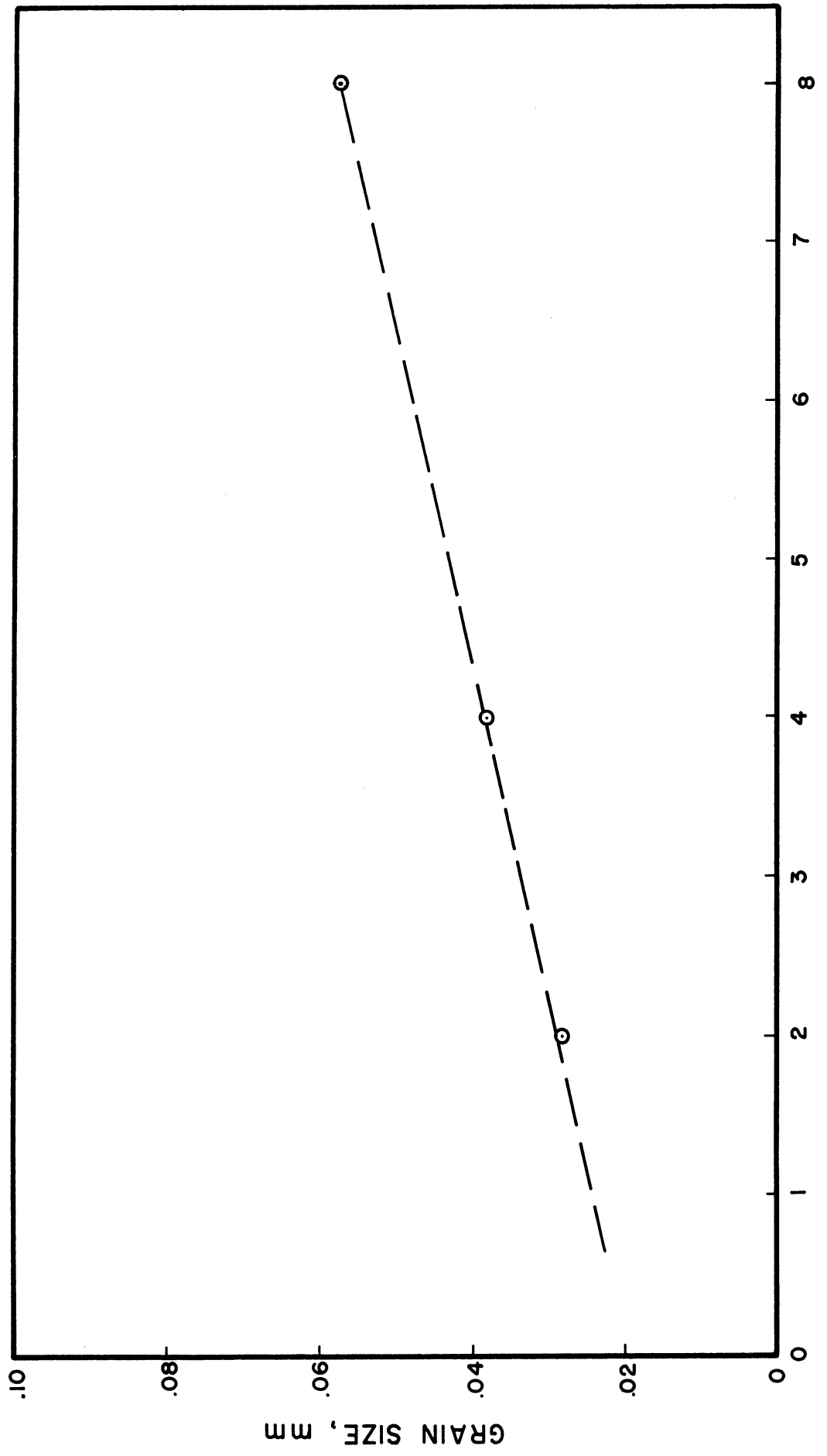

Figure 28. Grain Growth of Periclase (MgO) as a Function of Time in the Presence of a Calcium-Silicate Liquid at 1600°C.

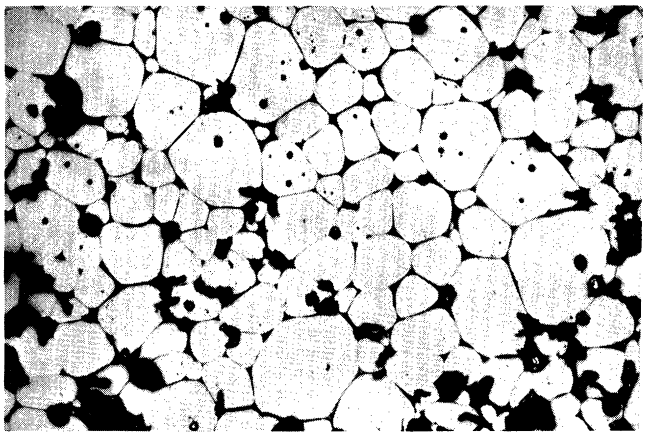

a) 4 hours.

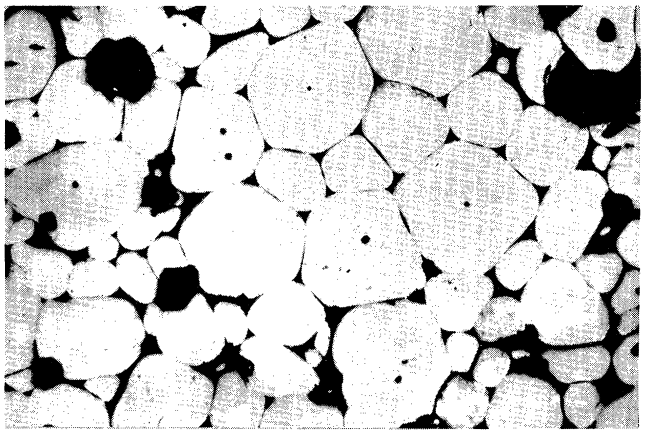

b) 16 hours.

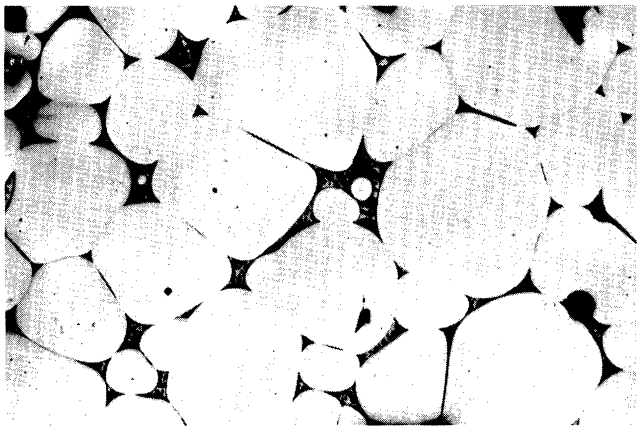

c) 64 hours.

Figure 29. Grain Growth of Periclase (MgO) as a Function of Time in the Presence of a CaO-Rich CaO-SiO_2 Liquid at 1600°C. Etched with 5% HF. 250X.

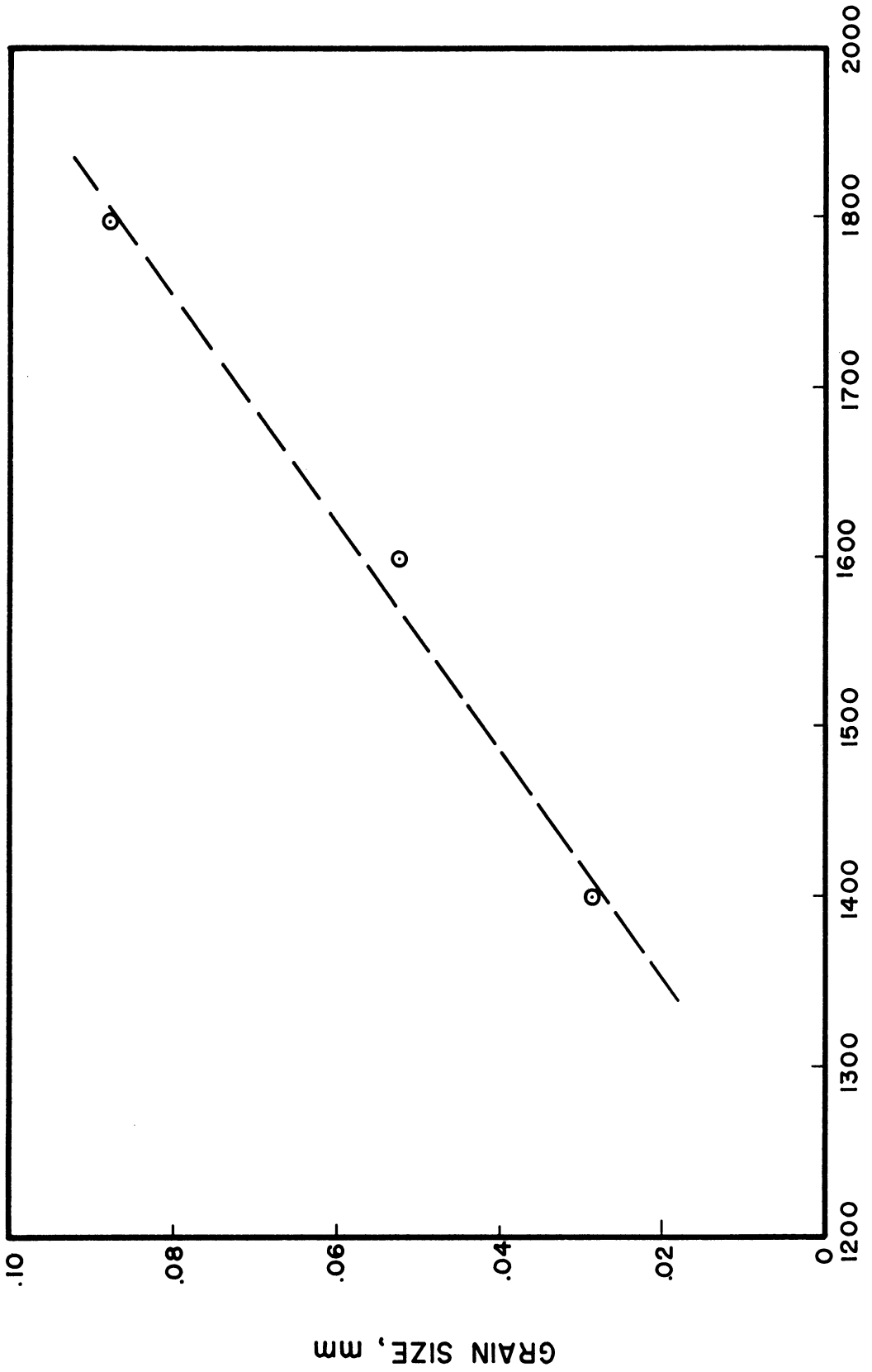

Figure 30. Grain Growth of Periclase (MgO) as a Function of Temperature After 4 Hours in the Presence of a $4CaO \cdot Al_2O_3 \cdot Fe_2O_3$-Rich Liquid.

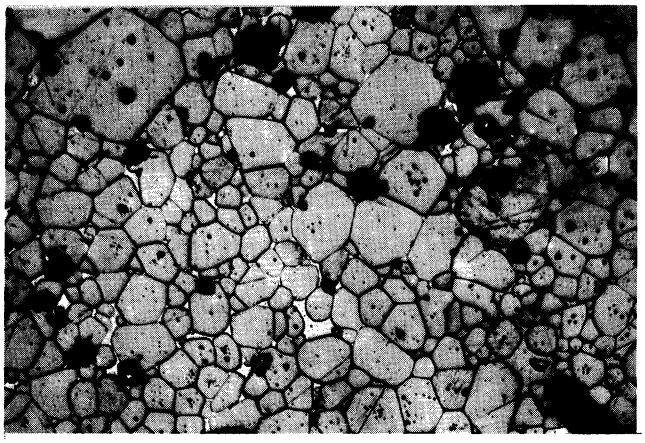

a) 1400°C.

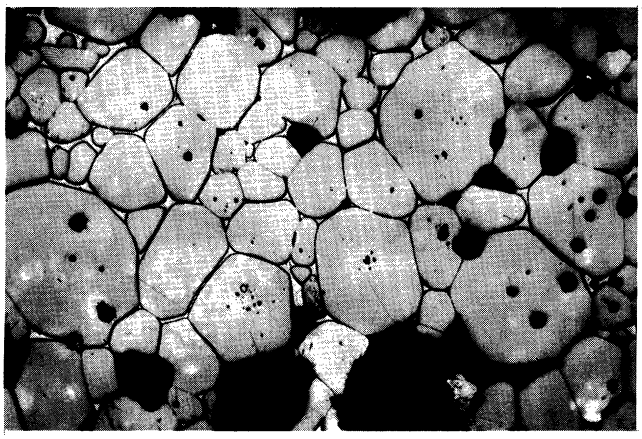

b) 1600°C.

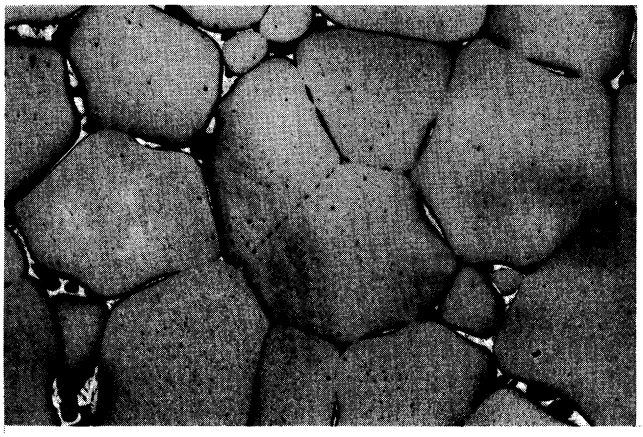

c) 1800°C.

Figure 31. Grain Growth of Periclase as a Function of Temperature After 4 Hours in the Presence of a $4CaO \cdot Al_2O_3 \cdot Fe_2O_3$-Rich Liquid. Etched with 5% HF. 250X.

CHAPTER V

DISCUSSION OF RESULTS

The pertinence of the results given in the previous chapter will be discussed and interpretations given where there seems to be need or justification for them. Where it may prove to be meaningful, and interesting correlation for the data will be presented.

1. Phase Geometry in Microstructures

A. Single Phase Molybdenum Metal

The results indicated that the true dihedral angle between grain boundary traces is very close to the expected value of 120 degrees. This is encouraging in that the measuring techniques and the method of handling the data, while not having been proved to be absolutely infallible, at least do not give an unreasonable or unexpected answer. It is suggested that the fit parameters of 3.59 and 3.63 obtained in processing the data are of the order of magnitude that one would desire for experimental data. Examination of Figure 3 should substantiate this point.

There may be some question about preferred orientation in a previously cold drawn wire, and it was in fact reported for molybdenum wire recrystallized at low temperatures by Taylor[48]. The fact that the true dihedral angle and fit parameter were very nearly identical in both the cross and longitudinal sections would lead to at least two possible conclusions. First, that preferred orientation did not persist at high temperatures after long annealing times where a substantial amount of grain growth and boundary migration have taken place, or

secondly, that preferred orientations even though present do not have a detectable effect on microstructure. The second conclusion would mean that grain boundary tensions are not sensitive to the orientation of the grains meeting to make up the boundary over the range of orientations that would be expected for the unknown degree of preferred orientation present.

B. Silicon-Aluminum Microstructures

Examination of the data for the silicon-aluminum system presented in Table IV will show a trend of decreasing dihedral angle with increasing temperature. Inspection of the phase diagram in Figure 5 will indicate that an increase in temperature from 600 to 1000°C will increase the solubility of silicon in the aluminum-rich liquid from 13 to 44 atomic percent. The fit parameters for the 600 and 1000°C samples are somewhat higher than would normally be desirable, however, it is obvious that a trend exists and the fact that it should be a detectable one is confirmed by the photomicrographs shown in Figure 6. The photomicrograph might also explain the high value of the fit parameter for the 1000°C sample. It is apparent that some precipitation has taken place in the liquid and in some cases it may be such as to obscure the real angle which existed at the higher temperature. Care was taken to avoid such situations during the measuring, however it is unlikely that complete success was attained.

C. Silicon-Tin Microstructures

Examination of the true dihedral angle data for the silicon-tin system shown in Table V will show that there is little if any real

change in the angle as the temperature is increased from 600 to 1000°C. The value reported for 600°C may be in question; however, the fact that the angle increases with time at temperature would indicate that the process of geometric equilibration has not been completed. This is very likely as there is little interaction between the solid and the liquid at this temperature. Inspection of the phase diagram reproduced in Figure 7 will confirm this point and will indicate that there is very little change in the solubility of silicon in the tin-rich liquid over the temperature range in question. When the data and phase relationships for both the silicon-aluminum and silicon-tin systems are compared it becomes apparent that a change in microstructure occurs with a change in temperature only when the change in temperature produces a significant change in the solubility of the silicon in the liquid phase.

Following the lead of Taylor[28], it was noticed that an interesting correlation could be found between the ratio of the solid/liquid interface energy and the solid/solid grain boundary energy, and the composition of the liquid phase. This ratio can be obtained from Equation (2) if the dihedral angle is known, and the composition of the liquid is read off the phase diagram. Table XIV gives the values of dihedral angle and temperature taken from Tables IV and V and values of the energy ratio and liquid composition for the silicon systems. Only the data at 1000°C is used from the silicon-tin system because it is thought that this is the most accurate and that this sample was more nearly geometrically equilibrated.

TABLE XIV

ENERGY RATIOS AND LIQUID COMPOSITIONS FOR SILICON SYSTEMS

Equilibration Temperature °C	True Dihedral Angle (Degrees)	Phase Boundary Energy / Grain Boundary Energy	Percent Silicon in Liquid
	Silicon-Aluminum Data		
1000	40	0.532	44
800	55	0.565	27
600	64	0.589	13
	Silicon-Tin Data		
1000	71	0.614	6

The correlation between the logarithm of the silicon content of the liquid and the ratio of the boundary energies is shown graphically in Figure 32. It is seen that the above correlation adequately describes and predicts the changes in microstructure for the silicon systems studied.

D. Nickel-Bismuth Microstructures

The summary of data presented in Table VI for the nickel-bismuth system is what is thought to be the best data from a number of samples equilibrated and from a larger number of sets of angle measurements. All of the measurements made are tabulated and discussed in Appendix B.

If the values for the true dihedral angles reported in Table VI are compared with the phase diagram reproduced in Figure 9, it will be noted that the decrease in angle is accompanied by an increase in the nickel content of the liquid as the temperature is raised. The

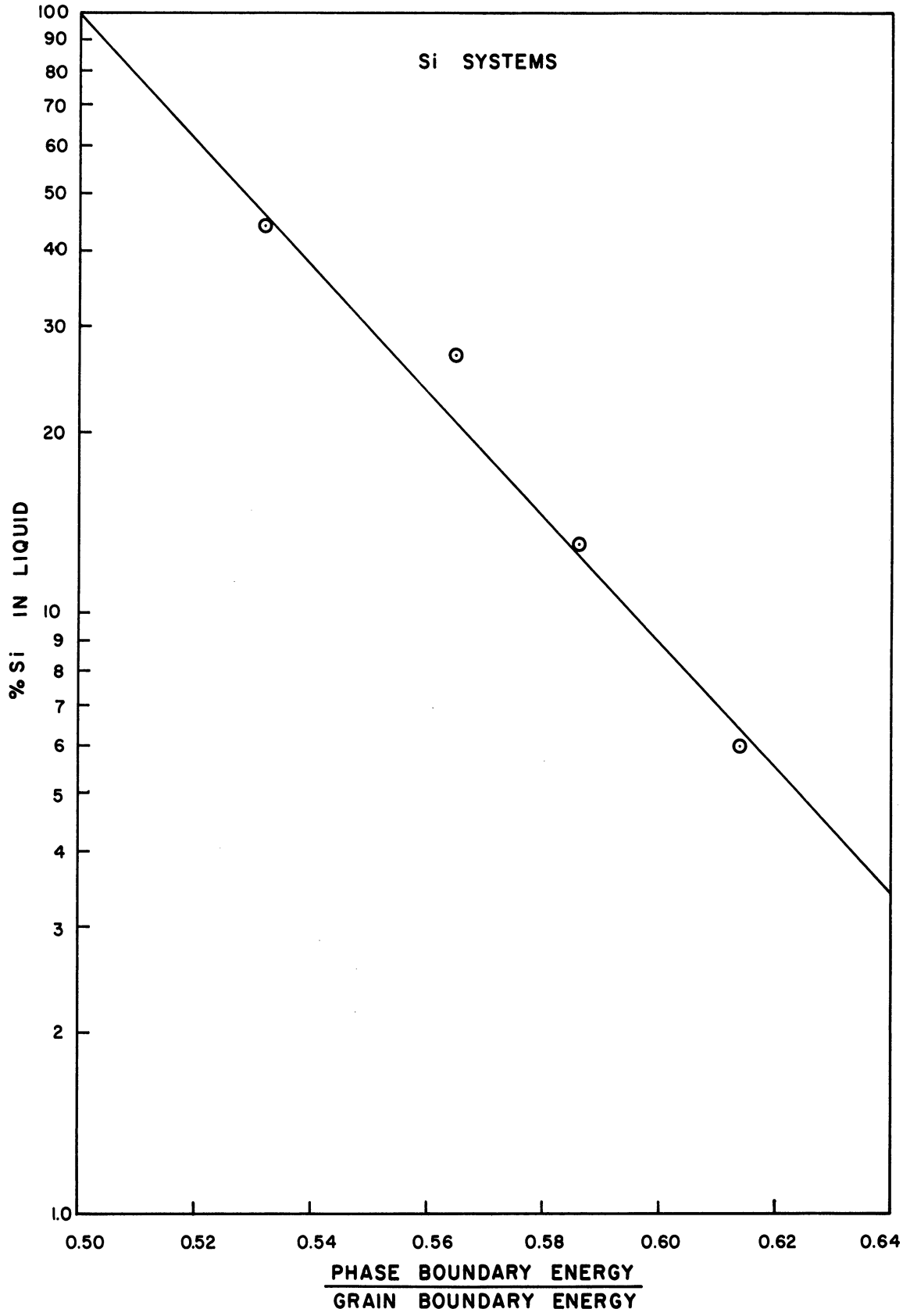

Figure 32. Logarithm of the Silicon Content of the Liquid vs. the Ratio of the Boundary Energies.

nickel content of the liquid increases from 25 atomic percent at 700°C to 33 atomic percent at 900°C as the angle decreases from 41 degrees to 27 degrees. This difference in structure is readily apparent in the photomicrographs shown in Figure 10.

The correlation shown in the preceding section is not given here because there are only three data points (two of which are very close together), and it is felt that extrapolation is not warranted with this limited amount of data.

E. Aluminum-Antimony Microstructures

Examination of the dihedral angle data shown in Table VII for the solid AlSb in equilibrium with both aluminum-rich and antimony-rich liquids, will reveal that there are significant changes in microstructure with temperature in both cases. This conclusion is substantiated by the photomicrographs shown in Figures 12 and 13. If attention is paid to the phase diagram in Figure 11, it will be noticed that there are also significant changes in the liquid compositions on both sides of the compound over the temperature range in question. In particular, it will be noticed that for aluminum-rich liquids the greatest change in microstructure occurred over the temperature interval of 900 to 1000°C and it is over this same temperature interval that the change in liquid composition is the greatest. The correlation between the ratio of the boundary energies and the liquid phase composition was found in this system also. Table XV gives a tabulation of the angle data and temperatures taken from Table VII, the ratio of the energy of the boundaries calculated through Equation (2) and the liquid compositions as read off

of the phase diagram. The correlation between the ratio of the boundary energies and the logarithm of the AlSb content of the liquid is shown graphically in Figure 33 for both the aluminum and antimony-rich liquids. This correlation adequately describes the changes in microstructure for either liquid with changes in composition.

TABLE XV

ENERGY RATIOS AND LIQUID COMPOSITIONS FOR THE ALUMINUM-ANTIMONY SYSTEM

Equilibration Temperature °C	True Dihedral Angle (Degrees)	Phase Boundary Energy / Grain Boundary Energy	Percent AlSb in Liquid
	Structures Equilibrated with Aluminum-Rich Liquids		
700	78	0.643	2
800	74	0.625	5
900	59	0.575	16
950	39	0.530	28
1000	25	0.511	45
	Structures Equilibrated with Antimony-Rich Liquids		
700	56	0.565	7
800	48	0.547	20
900	38	0.528	37
950	31	0.518	48
1000	27	0.514	63

If comparisons are made between microstructures with liquids on either side of the compound at the same temperature, it will be found that at every temperature except 1000°C, the dihedral angle is smaller for the

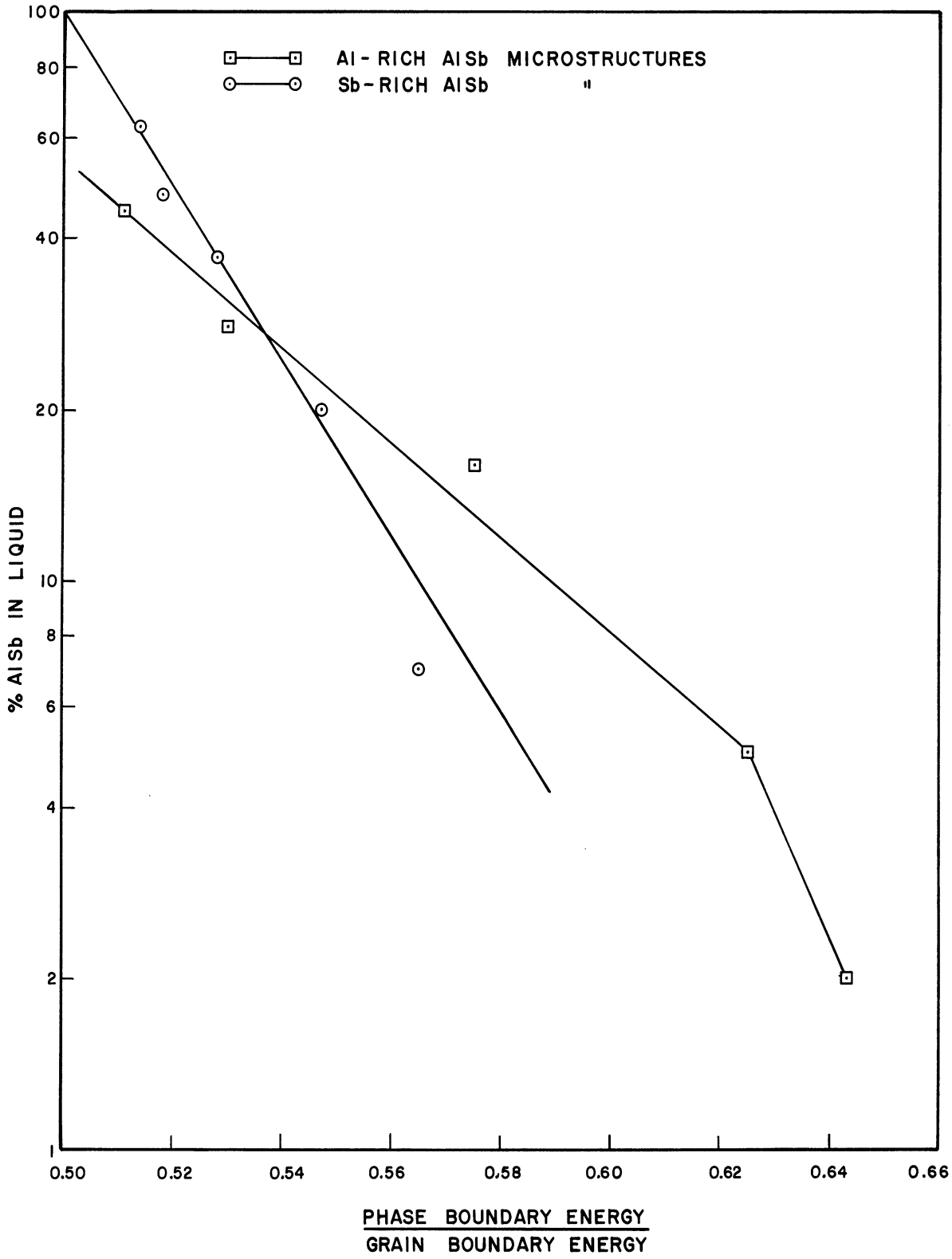

Figure 33. Logarithm of the AlSb Content of the Liquid versus the Ratio of the Boundary Energies.

antimony-rich liquids. It will also be noted that the solubility of the solid AlSb is higher in every case in the antimony-rich liquids. As is seen in Figure 33, however, the rate of change in the microstructures is different for the two liquids. No definite explanation for this difference can be given at the present time except to note that a theory developed by Wagner[49] may give some insight and meaning to the liquid phases in question. Briefly stated, this theory says that for intermetallic compound forming systems, the liquids in equilibrium with these compounds are more ordered when the solubility of the solid is high at temperatures below the melting point of the compound. This situation may be spotted on the phase diagram where very steep liquidus lines correspond to highly ordered liquids and the rather flat liquidus lines correspond to nearly ideal liquids in which the two kinds of atoms are distributed at random.

Schottky and Bever[50] have applied Wagner's theory to several III-V compound forming systems. They found that liquids in the indium-antimony system give slight negative deviations from the ideal liquid, indicating some ordering. However, liquids in the gallium-antimony system were reported to be very near ideal indicating that the atoms in these liquids must be distributed at random. These comparisons were made using an equation derived by Wagner[49] to calculate the liquidus for an ideal liquid in equilibrium with the compounds, and comparing this to the actual liquidus curve.

If the ideal liquidus lines are calculated for the aluminum-antimony system according to a suggestion made by Schottky and Bever[50],

and then compared to the actual liquidus lines, as shown in Figure 11, it is found that the aluminum-rich liquids are very nearly ideal. It is expected, however, that the antimony-rich liquids would be more ordered because these liquids dissolve more of the compound AlSb than the ideal liquid. The only assumption necessary to calculate the ideal liquidus is that the entropy of fusion of AlSb is 6.15 cal/g atom/°C, which is the same as that for GaSb as determined by Schottky and Bever. This assumption is reasonable since the two compounds have the same crystal structure and other similar properties.

When the important assumption is made that the grain boundary energy is the same when the solid is in equilibrium with liquids on either side of the compound, then it would appear that the ordered antimony-rich liquid allows for a lower energy solid/liquid interface. This point will be discussed in the next two sections.

F. Tin-Tellurium Microstructures

If the tin-tellurium dihedral angle data presented in Table VIII are viewed in light of the phase diagram reproduced in Figure 14, it will become apparent that significant changes in the microstructure occur with temperature only when the temperature change produces a substantial change in the solubility of the solid SnTe in the liquid phase present. Photomicrographs which illustrate the change in the degree of liquid penetration of grain boundaries are shown in Figures 15 and 16. Of particular significance is the fact that for tin-rich liquids there is no detectable change in the microstructure over the temperature range from 300 to 550°C, while there is a marked change in

microstructure over the short temperature interval from 600 to 700°C. Inspection of the phase diagram will show that the solubility of the solid SnTe in the liquid varies only from 1 to 6 percent over the first temperature interval, but varies from 10 to 40 percent over the second interval. For tellurium-rich liquids there is a continuous change in microstructure over the temperature interval from 450 to 600°C and this is accompanied by a continuous change in the solubility of SnTe in the liquid.

The correlation between the microstructure and the composition of the liquid phase was found in this system also, but it is not as good as the ones already reported. A tabulation of the temperatures and dihedral angles from Table VIII along with the necessary data from the phase diagram and the calculated energy ratios is given in Table XVI. This correlation is shown graphically in Figure 34 for both the tin-rich and tellurium-rich structures.

From Figure 34 it is seen that the rate of change of the microstructure with composition is different for the two liquids considered. If we again apply the Wagner theory, we are led to the conclusion that the tellurium-rich liquids are more ordered than the tin-rich liquids because they dissolve more of the SnTe solid. By comparison of the data in Table VIII it is found that at a given temperature the tellurium-rich liquids will penetrate SnTe grain boundaries more extensively than tin-rich liquids. When the previous important assumption is made that the grain boundary energy is the same with the two different liquids, the conclusion may again be reached that the ordered tellurium-rich liquid gives rise to a lower solid/liquid interface energy.

TABLE XVI

ENERGY RATIOS AND LIQUID COMPOSITIONS FOR THE TIN-TELLURIUM SYSTEM

Equilibration Temperature °C	True Dihedral Angle (Degrees)	Phase Boundary Energy / Grain Boundary Energy	Percent SnTe in Liquid
	Structures Equilibrated with Tin-rich Liquids		
300	77	0.640	1
450	79	0.646	2
500	74	0.625	4
550	77	0.640	6
600	63	0.486	10
650	61	0.580	20
700	46	0.542	40
	Structures Equilibrated with Tellurium-rich Liquids		
450	58	0.573	38
500	47	0.545	46
550	45	0.540	54
600	39	0.530	62

The data fitting parameter for the tin-tellurium alloys is found to be consistantly higher than for aluminum-antimony alloys. There is no apparent explanation for this behavior except that there might be more anisotropy in the grain boundary energies for the SnTe solid. This might be possible because SnTe has the sodium chloride crystal structure which is of higher symmetry than the zinc blend

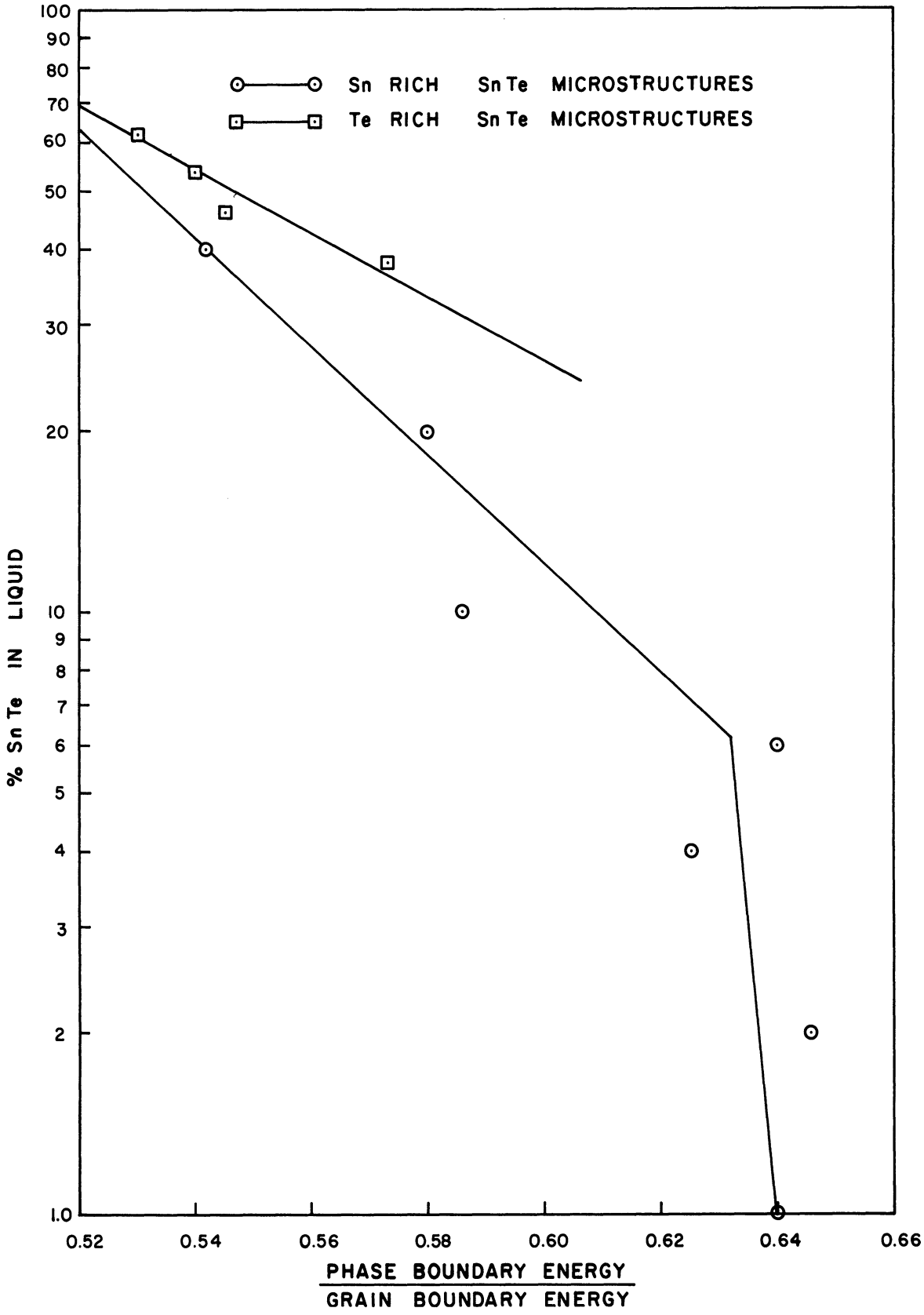

Figure 34. Logarithm of the SnTe Content of the Liquid versus the Ratio of the Boundary Energies.

structure of the AlSb. The higher symmetry of the crystal structure would allow for more special or favored low energy orientations between adjacent crystallites. The overall effect of this situation would be to have a range of true dihedral angles existing in the microstructure rather than the one true angle which has been assumed in developing the theoretical curves. This in turn would lead to a greater spread in the values of angles actually observed in a microstructure.

G. Magnesium-Antimony Microstructures

The reason for studying the microstructures in the magnesium-antimony system was to investigate microstructures developed in the presence of highly "ordered" liquids. From Wagner's theory, one would expect the liquids in a system such as this to possess more order since they dissolve large quantities of the compound well below its melting point. (See phase diagram in Figure 17.) Examination of the data in Table IX will show that there is a marked change in microstructure over the temperature interval 600 to 700°C. This conclusion is also supported by the photomicrographs shown in Figure 18. Inspection of the phase diagram will indicate that there is a marked change in the solubility of the solid Mg_3Sb_2 in the liquid over this same temperature interval. As has been the case for the other systems discussed, the change in microstructure with temperature in this system is accompanied by a change in the solubility of the solid in the liquid. Another significant point here is the fact that a liquid which penetrates the solid grain boundaries rather deeply is formed some 500°C below the melting point of the solid. This is in contrast to the two intermetallic compound

forming systems discussed previously where a comparable degree of penetration was not found until temperatures within 100°C of the melting point of the compound were reached. On the limited amount of evidence in this system, it might be suggested that a more highly ordered liquid (i.e., one which dissolves more of the solid in compound-forming systems) will lead to a higher degree of liquid penetration of the solid grain boundaries and this is presumably due to a lower energy solid/liquid interface between the solid and the ordered liquid.

H. Aluminum-Indium-Antimony Microstructures

The reason for studying microstructures in the aluminum-indium-antimony system was to determine the effect of a third component on structures already discussed in the two component aluminum-antimony system. The compositions for the liquids in equilibrium with the solid AlSb are shown on the ternary diagram in Figure 19 and are to be considered as only approximate, since they were determined from aim compositions of the ingots melted, and x-ray diffractometer patterns of the surface of equilibrated samples. A difference in the appearance of the liquid phase is also apparent in the photomicrographs in Figure 20. The data in Table X should be compared with that for aluminum-antimony samples in Table VII. In particular, if the In-Sb-rich samples at 700 and 800°C are compared with the antimony-rich structures at the same temperatures, it will be found that there is essentially no difference. It will be recalled that the suggestion was made that antimony-rich liquids are more ordered than an ideal liquid with the component atoms distributed at random. If there is to be any ordering in the liquid phase in the

ternary system, it would certainly be expected to occur in liquids of the In-Sb-rich composition, because these liquids exist just above the compound InSb which forms as the solid at lower temperatures. Before making direct comparisons between boundary energies in the binary and ternary systems, it should be pointed out that there is a possibility for some slight amount of solid solution of indium in the AlSb solid and there is also the possiblity of adsorption of indium in the AlSb grain boundaries. If the important assumption is made that these effects are negligible or have a negligible effect on the AlSb grain boundary energy, then these experiments would be evidence in support of the hypothesis that the antimony-rich liquids are somewhat ordered and that this situation leads to a lower solid/liquid interface energy.

A comparison of the data at 800°C for the aluminum-rich and Al-In-rich liquids indicates that the addition of indium to the liquid increases the amount of penetration of solid AlSb grain boundaries. Here the possibilities of solid solution or grain boundary adsorption of the indium cannot interfer with our interpretation because both of these processes are expected to lower the grain boundary energy. This would lead to an increase in the dihedral angle and not the decrease which is observed. Examination of the ternary diagram will show that the addition of indium to an aluminum-rich liquid will slightly increase the solubility of AlSb in the liquid. It is therefore suggested that by increasing the solubility of AlSb, indium additions make the structure of the liquid more nearly like that of the solid and thereby lower the solid/liquid interface energy. This interpretation is in line with

the results of Schottky and Bever[50] which were discussed in the section on aluminum-antimony microstructures.

I. Periclase (MgO) Microstructures

The microstructures developed by periclase (MgO) in the presence of various oxide liquids are of interest because of their industrial importance as steel-making furnace refractories and because it is known that these refractories can become very weak in the presence of low liquid contents at temperatures well below the melting point of the solid.

Examination of the summary of periclase (MgO) dihedral angle data presented in Table XI will show that several comparisons can be made.

(1) Within a given ternary system, for example the CaO-MgO-Al_2O_3 system, there is not significant change in microstructure in going from a CaO-rich to an Al_2O_3-rich liquid at a given temperature.

(2) It should also be noted that there is no significant change in microstructure in the CaO-MgO-SiO_2 ternary in going from a SiO_2-rich to a CaO-rich liquid.

(3) If the microstructures found in the CaO-MgO-Al_2O_3 ternary are compared at 1500 and 1600°C, it will also be noted that there is no significant change over this temperature range.

(4) If the microstructures found in the CaO-MgO-Al_2O_3 ternary are compared with those found in the CaO-MgO-SiO_2

ternary at 1600°C, it will be seen that, for the compositions studied, the liquids containing SiO_2 penetrate periclase (MgO) grain boundaries more extensively, producing a smaller dihedral angle.

(5) If the microstructures containing the $4CaO \cdot Al_2O_3 \cdot Fe_2O_3$-rich liquid are compared with those formed in the $CaO-MgO-Al_2O_3$ ternary, it will be found that the addition of Fe_2O_3 to the liquids formed in the above ternary has no significant effect on the microstructure of periclase (MgO).

In summary then, it may be pointed out that liquids which contain SiO_2 will form microstructures with more penetrating liquids than any of the other compositions studied. Although no definite explanations for this microstructural behavior can be given at this time, several possible explanations which seemed to be useful in our previous discussions will be discussed.

The known equilibrium phase relationships provide little information which may explain this behavior. In the $CaO-MgO-Al_2O_3$ ternary, there is very little change in the solubility of MgO with composition along either the 1500 or 1600°C isotherms, nor is the change in solubility with temperature very large. Recently, Kalyanram and Bell[51] have reported measured activities in this ternary. At 1500°C, the activity of CaO and Al_2O_3 were reported to be 0.8 and 0.01 respectively for a liquid corresponding to the CaO-rich Al_2O_3-CaO liquid in Table XI. Similarly, the activities for a liquid corresponding to the Al_2O_3-rich Al_2O_3-CaO composition were reported to be 0.15 and 0.20 for CaO and Al_2O_3

respectively. At 1600°C, about the same variations in activity would be expected. It would appear then that the activities of CaO and Al_2O_3 do not control the solid/liquid interface energy over this range. Since the possibilities outlined above do not lead to positive interpretations, it might be suggested that a change in microstructure would not be expected in this system because the solubility of MgO is not affected by the CaO/Al_2O_3 ratio of the liquid.

In the $CaO-MgO-SiO_2$ ternary the situation is somewhat different. From the data in Table XI it is seen that there is very little if any change in microstructure within the limits of liquid compositions studied in this system. Inspection of the phase diagrams reproduced in Figure 21 will show that the solubility of MgO in the liquid changes significantly with liquid composition along the 1600°C isotherm. Closer examination will reveal, however, that this isotherm is parallel to and almost directly above the join from forsterite ($2MgO \cdot SiO_2$) to di-calcium silicate ($2CaO \cdot SiO_2$) with the compounds monticellite ($CaO \cdot MgO \cdot SiO_2$) and merwinite ($3CaO \cdot MgO \cdot 2SiO_2$) in between. With these compounds and ranges of solid solution for them along this line, it seems logical to suggest that the structure of the liquids encountered along the 1600°C isotherm are very similar. The structure of these silicate liquids has in fact been reported by Richardson[52] to be essentially constant. This conclusion is based on both x-ray studies and viscosity data for silicate melts in the orthosilicate composition range. The structure of the liquids is controlled primarily by the SiO_4 tetrahedra, with the divalent metallic ions being shared at the corners of the

tetrahedra. Over the range of compositions of these liquids then, on an atomistic scale, this would mean that magnesium ions are replacing calcium ions in a CaO-MgO-SiO_2 type liquid, whose structure is controlled by the $SiO_4^{=}$ ion. A more satisfactory explanation or more supporting data are not available at this time. From the data in Table XI, it is also seen that the addition of Fe_2O_3 to a CaO-Al_2O_3 liquid does not alter the microstructure. This system is a little too cumbersome to analyze except to note in the phase diagram reproduced in Figure 23, that the liquid in equilibrium with the solid does not dissolve much of the MgO.

2. Grain Growth

The growth of solid grains in solid-liquid composite structures has received very little attention. The fact that marked differences in the mode of growth occur with different materials is worth noting, and inspection of the as-solidified structures shown throughout this report will substantiate this point. The effects of extended time at higher temperatures, where in this case a liquid phase is developed, should also be of interest. Changes which occur under such a condition are shown pictorially in Figure 26 for AlSb grains in equilibrium with an antimony-rich liquid. It appears that the initial euhedral outlines of grains in the as-solidified structure are the result of anisotropic growth rates for different crystal faces. The important effects of interfacial tensions are seen as anhedralization takes place as the structure undergoes geometric equilibration. This process is seen to produce a rounding of sharp corners, development of definite dihedral

angles of the liquid in contact with a grain boundary, and a gradual reduction of the total solid-liquid interfacial area and thereby reducing the total energy.*

Examination of the SnTe as-solidified structures will reveal a basic difference in the mode of growth of the individual crystallites. They are equiaxed and this may be directly attributed to the high symmetry of their sodium-chloride structure. The effect of time on the size of the grains is striking when the as-solidified structure is compared to a sample equilibrated for 4 hours at 500°C. This initial growth may be attributed to the driving force of the reduction of interfacial free energy by decreasing the solid-liquid interface area. With more time, the rate of growth becomes vanishing small, as seen in the 96 hour sample, and it is suspected that at this point the liquid channels become barriers to growth, much the same as inclusions are known to impede grain growth in metals. There is still present, however, the interfacial free energy driving force which will tend to minimize the total solid-liquid interface area.

The effect of interfacial free energy as a driving force for grain growth is apparent in the grain growth data for periclase presented in Table XII. This same data is shown graphically in Figure 28 where the average grain diameter is plotted against the square root of time. Since this correlation is the one to be expected from Equation (3), one may

*The reduction of the solid-liquid interfacial area is accompanied by an increase in the solid-solid grain boundary area. Since measurements of the amount of the two kinds of boundary areas were not made, it is not possible to prove conclusively which energy is responsible for the increase in grain size.

conclude that the primary driving force is the reduction of the interfacial free energy which accompanies an increase in grain diameter by decreasing the interfacial area. The higher growth rate for MgO in contact with a SiO_2-rich CaO-SiO_2 liquid than for the CaO-rich liquid may be explained in terms of the higher solubility of MgO in the first liquid. If liquid phase transport is the mechanism involved, then the diffusion rate would be higher for a liquid with a higher MgO content.

Examination of the periclase (MgO) grain growth data versus temperature presented in Table XIII and shown in Figures 30 and 31 will reveal that the rate of grain growth increases markedly with increasing temperatures. There may be at least two reasons for this increase. First, the $4CaO \cdot Al_2O_3 \cdot Fe_2O_3$-rich liquid dissolves more of the solid (see Figure 23) at higher temperatures and, as cited in the previous paragraph, this can lead to faster growth rates. The second and probably more influential factor is that at higher temperatures, the mobilities of the magnesium and oxygen ions are higher, allowing for faster diffusion from the small grains, through the liquid, and onto the growing grains.

CHAPTER VI

CONCLUSIONS

The following conclusions may be drawn from this work:

1. Angle measuring and data processing techniques were validated by giving the expected value for the true dihedral angle in a well annealed molybdenum single phase microstructure.

2. A change in microstructure accompanying a change in temperature was found to occur only when the change in temperature produces a substantial change in the solubility of the solid in the liquid, for the wide variety of metallic and intermetallic compound forming systems studied.

3. A correlation between the logarithm of the solubility of the solid in the liquid and the ratio of the solid/liquid interface energy and the grain boundary energy of the solid was found to hold within a given two-phase region for the metallic and intermetallic compound forming systems studied.

4. Indications that an "ordered" liquid can form a low energy solid/liquid interface were found in all of the intermetallic compound forming systems studied.

5. The composition of the liquid phase was found to have only a secondary effect on the microstructures containing solid periclase (MgO). Indications are that ordering in the liquid phase may be controlling microstructures in this case.

6. The effect of interfacial free energy as a driving force for grain growth was found in both solid-liquid microstructures containing intermetallic compounds as the solid phase, and periclase (MgO) as the solid phase.

7. The rate of grain growth of periclase (MgO) was found to increase markedly with increasing temperature.

APPENDIX A

DIHEDRAL ANGLE MEASUREMENTS

The problem of measuring dihedral angles is, like any quantitative metallographic technique a statistical problem because we are trying to measure a feature which is really a three-dimensional structure from traces of that feature on a two-dimensional plane. Harker and Parker[1] have derived the mathematical expression (Equation 1) which relates the probability of seeing a feature in the two-dimensional plane to its existance in three-dimensions. Experience has shown that a number of factors can influence the accuracy and meaning of angle measurements.

In addition to the accuracy of the individual measurements as discussed in Chapter III, the actual measurement can be influenced by bias on the part of the observer. This can operate in two ways; first, the observer can subconsciously overlook angles which are either larger or smaller than he thinks they should be, or secondly, he can prejudice the measurements he does make. It is thought that the best guard against bias is to have an impartial observer do some measuring as a check.

The surface condition of the specimen to be measured is of utmost importance. Errors can arise here from having an inclusion which is of a different hardness than the material proper, as this situation can lead to relief polishing. Care must be taken in polishing to maintain a flat surface if reliable and reproducable measurements are to be obtained.

Since measuring dihedral angles is a statistical problem, errors can arise from just having a "bad" sample. Riegger and Van Vlack[3] have calculated the probable accuracy for a given true dihedral angle for 25 and 100 measurements. This accuracy may be compared with experimental angle data from the cross section of the molybdenum sample. Here the data was processed in batches of 25 angles, and the results are presented below. The fit parameter is an indication of the deviation of the measurements from the theoretical distribution. It is found by experience that when the parameter is less than 5.00, the fit is as good as should be expected from experimental data.

SUMMARY OF MOLYBDENUM CROSS SECTION DATA

Number of Angles	True Dihedral Angle (Degrees)	Fit Parameter
First 25	116	5.02
Second 25	123	4.21
Third 25	119	5.40
Fourth 25	122	4.89
Fifth 25	121	6.57
Sixth 25	113	4.30
Total 150	120	3.59

According to Riegger and Van Vlack, for 25 angle measurements, the accuracy to be expected is $\pm$ 4° in 68 percent of the cases for a true dihedral angle of 120°. If the true dihedral angle for the single phase solid is 120°, then the measurements may be considered to be statistically

accurate, since only one of the six batches differs from 120° by more than 4°.

The amount of second phase material present in a structure may influence the accuracy of measurements by, first being present in such small quantities that the chance of seeing enough measurable angles on a random basis is seriously affected, or secondly, by being present in such large amounts that the chance of seeing enough grain boundaries in the solid on a random basis is affected. There is obviously then a large range of inclusion contents which will facilitate angle measurement between the two extremes just cited. Examples which tend to substantiate this contension are shown below in the form of data from aluminum-antimony samples which differed in composition and therefore in liquid content.

In comparing the following data, it will be noted that there is no consistant nor statistically significant variation in the true dihedral angle measured with the amount of liquid. Another interesting fact to note is that three of the four sets of data (19%Al - 81%Sb at 700°C, 17.5%Al - 82.5%Sb at 700°C, 17.5%al - 82.5%Sb at 800°C, and 15%Al - 85%Sb at 900°C) for which the calculated true dihedral angle differed significantly from that for all samples at one temperature, had fit parameters which were considerably higher than the rest of the samples in the table. This high fit parameter may serve as a warning that something may be wrong with a particular set of angle measurements.

Application of the above methods of analysis depends upon the important assumption that there is a true dihedral angle within the structure being investigated. It is felt that this condition is usually

SUMMARY OF ALUMINUM-ANTIMONY ANGLE DATA AT VARIOUS ANTIMONY-RICH LIQUID LEVELS

Sample Composition	Equilibration Temperature °C	Time (Hours)	Number of Angles	True Dihedral Angle (Degrees)	Fit Parameter
19% Al-81% Sb	700	100	50	60	9.43
17.5% Al-82.5% Sb	700	100	50	49	13.60
15% Al-85% Sb	700	100	50	55	4.79
12.5% Al-87.5% Sb	700	100	50	55	5.11
All Sb-rich	700	100	200	56	4.82
17.5% Al-82.5% Sb	800	72	50	45	4.52
15% Al-85% Sb	800	72	50	50	2.61
12.5% Al-87.5% Sb	800	72	50	49	4.27
All Sb-rich	800	72	150	48	3.00
11.5% Al-82.5% Sb	900	48	50	40	5.19
15% Al-85% Sb	900	48	50	33	12.20
12.5% Al-87.5% Sb	900	48	50	39	5.37
All Sb-rich	900	48	150	38	3.65
11.5% Al-82.5% Sb	950	46	25	29	5.29
15% Al-85% Sb	950	24	50	32	4.12
15% Al-85% Sb	950	4	50	29	6.00
All Sb-rich	950		125	31	4.76

met in solid-liquid structures if enough time has been allowed at the higher temperature to allow the structure to come to geometric equilibrium. The time required for geometric equilibrium is usually considerably longer than

for ordinary chemical equilibrium. The experienced observer can ascertain when geometric equilibrium has been obtained by the appearance of well defined angular junctions between grain boundaries and solid/liquid boundaries. As an example, the geometry of the liquid phase in the as-solidified structures shown in the chapter on results should be compared with the shapes of the quenched liquid inclusions in the equilibrated microstructures.

APPENDIX B

ORIGINAL DATA FOR NICKEL-BISMUTH SYSTEM

Because of the difficulty involved in obtaining good data in the nickel-bismuth system, all of the angle measurements made and the conditions under which they were made are tabulated below.

SUMMARY OF NICKEL-BISMUTH ANGLE DATA

Equilibration Temperature °C	Time (Hours)	Number of Angles	True Dihedral Angle (Degrees)	Fit Parameter	Remarks
700	74	50	41	10.90	Diamond polished and etched
900	24	75	45	8.70	with D-4.
700	74	100	38	3.71	Repolished and etched very
700	96	100	41	5.95	lightly with D-4.
900	24	50	38	5.17	
700	48	100	39	4.74	New samples polished on
900	12	100	36	7.14	Linde "B" Syntron and
1100	2	100	48	7.04	measured unetched.
700	74	50	41	4.12	Repolished on Linde "B" Syn-
900	24	50	28	3.67	tron and measured along edge of sample.
1000	2	100	27	5.05	Samples polished on Linde
1100	1	100	27	7.57	"B" Syntron and measured along
1190	1	50	39	5.15	edge of specimen

Samples in this system were very difficult to polish because both the nickel-rich solid phase and the bismuth-rich quenched liquid phase are very soft and easily smeared. What is thought to be the "real" structure was not revealed until after the sample had been mechanically polished for 2-3 hours on the Linde "B" Syntron. The first measurements made on these samples showed that the dihedral angle increased with increasing temperature until at 1100°C it was appreciably larger than at 700°C. The initial measurements were made on a random selection basis over the entire surface of the specimen. Closer examination of the structures, however, revealed that the dihedral angle varied from the edge of the specimen to the interior on samples quenched from higher temperatures. In fact, the interior of the sample quenched from 1190°C very closely resembled that of the as-solidified structure. This situation was not the case for the samples quenched from 700°C, as a comparison of the numbers will show. It was therefore concluded that the problems lay in the inability to quench in the equilibrated structure on samples heated to high temperatures in this system. For this reason, measurements were made along the edge of the sample where the cooling rate should be the fastest. It is thought that the values reported in Table VI are a close approximation to the true structure in these alloys.

Examination of the data will show the consistency of the data for measurements on samples equilibrated at 700°C. Close microscopic examination of the last five samples listed showed that the microstructure varied from surface to the interior of the specimen on all but the 700°C samples. The fact that the interior of the 1190°C sample had a structure

closely resembling that of the as-solidified ingot, was considered to be strong evidence pointing to a problem in quenching the sample fast enought to maintain the high temperature structure. If this is the case, then one would have to put less trust in the reliability of the figures for dihedral angles obtained even along the edge of the specimens equilibrated at 1000, 1100 and 1190°C. These structures may at best be in dynamic equilibrium while being quenched, and the rate of change would be expected to be higher for samples quenched from a higher temperature.

BIBLIOGRAPHY

1. D. Harker and E. R. Parker, "Grain Shape and Grain Growth," Trans. ASM, 34, (1945) 156.

2. Cyril Stanley Smith, "Grains, Phases, and Interfaces: An Interpretation of Microstructure," Trans. AIME, 175, (1948) 15.

3. O. K. Riegger and L. H. Van Vlack, "Dihedral Angle Measurement," Trans. AIME, 218, (1960) 933.

4. W. M. Williams and C. S. Smith, "A Study of Grain Shape in an Aluminum Alloy and Other Applications of Stereoscopic Microradiography," Trans. AIME, 194, (1952) 755.

5. K. K. Ikeuye and C. S. Smith, "Studies of Interface Energies in Some Aluminum and Copper Alloys," Trans. AIME, 185, (1949) 762.

6. L. H. Van Vlack, "Intergranular Energy of Iron and Some Iron Alloys," Trans. AIME, 191, (1951) 251.

7. L. H. Van Vlack, R. J. Warrick, J. M. Dahl, and O. K. Riegger, "Sulfide Inclusions in Steel," Trans. AIME, 221, (1961) 220

8. L. H. Van Vlack, "The Microstructure of Silica in the Presence of Iron Oxide," J. Am. Cer. Soc., 43, (1960) 140.

9. R. Shuttleworth, "The Surface Tension of Solids," Phys. Soc.,,63, (1950) 444.

10. R. L. Fullman, "Boundary Migration During Grain Growth," Metal Interfaces, ASM publication, (1952), 179.

11. P. A. Beck, J. C. Kremer, L. J. Demer, and M. L. Hotzworth, "Grain Growth in High Purity Aluminum and in an Aluminum - Magnesium Alloy," Trans. AIME, 175, (1948) 372.

12. J. C. Fisher, Private Communication to R. L. Fullman, Metal Interfaces, ASM publication, (1952) 183.

13. J. E. Burke, "Recrystallization and Sintering in Ceramics," Ceramic Fabrication Processes, New York, John Wiley and Sons, (1958) 120-131.

14. W. D. Kingery, "Densification During Sintering in the Presence of a Liquid Phase. I. Theory," J. Appl. Phys., 30, (1959) 301-306.

15. L. H. Van Vlack and O. K. Riegger, "The Microstructure of Magnesiowüstite [(Mg, Fe) O] in the Presence of SiO_2," Trans. AIME, 224, (1962).

16. E. Voce and A. P. C. Hallowes, "The Mechanism of the Embittlement of Deoxidized Copper by Bismuth," J. Inst. of Metals, 73, (1947) 323.

17. T. H. Schofield and F. W. Cuckow, "The Microstructure of Wrought Non-Arsenical Phosphorus - Deoxidized Copper Containing Small Quantities of Bismuth," J. Inst. of Metals, 73, (1947) 337.

18. D. A. Kraai, Effects of Some Liquid Metal Environments on the Fracture of Copper, Ph.D. Thesis, The University of Michigan, 1960.

19. C. E. Sims and G. A. Lilliequist, "Inclusion - Their Effect, Solubility, and Control in Cast Steels," Trans. AIME, 100, (1932) 154.

20. C. Benedicts and H. Lofquist, Nonmetallic Inclusions in Iron and Steel, John Wiley and Sons, New York, (1931).

21. R. G. Wells and L. H. Van Vlack, "Mineral and Chemical Changes in Periclase Brick Under Conditions of Steel Plant Operation," Journ. Amer. Ceram. Soc., 34, (1951) 64.

22. J. C. Borland, "Suggested Explanation of Hot Cracking in Mild and Low Alloy Steel Welds," British Welding Journal, 8, (1961) 526.

23. R. C. Talman, "Consideration of the Gibbs Theory of Surface Tension," J. Chem. Phys., 16, (1948) 758.

24. J. W. Gibbs, Collected Works, Vol. 1, New Haven, Yale University Press, (1948) 224.

25. E. A. Guggenheim, "The Thermodynamics of Interfaces in Systems of Several Components," Trans. Faraday Soc., 36, (1940) 397.

26. J. W. Cahn and J. E. Hilliard, "On the Equilibrium Segregation at a Grain Boundary," Acta Met., 7, (1959) 219.

27. J. W. Cahn and J. E. Hilliard, "Grain-Boundary Energies in Gold-Copper Alloys," Acta Met., 8, (1960) 26.

28. J. W. Taylor, "An Evaluation of Interface Energies in Metallic Systems," J. Inst. of Metals, 86, (1957-58) 456.

29. A. S. Skapski, "The Temperature Coefficient of the Surface Tension of Liquid Metals," J. Chem. Phys. 16, (1948) 386.

30. B. C. Allen and W. D. Kingery, "Surface Tension and Contact Angles in Some Liquid Metal - Solid Ceramic Systems at Elevated Temperatures," Trans. AIME, 215, (1959) 30.

31. A. S. Skapski, "A Theory of Surface Tension of Solids - I. Application to Metals," Acta Met, 4, (1956) 576.

32. J. E. Hilliard and J. W. Cahn, "On the Nature of the Interface Between a Solid Metal and Its Melt," Acta Met, 6, (1958) 772.

33. J. W. Taylor, "The Surface Tensions of Liquid - Metal Solutions," Acta Met, 4, (1956) 460.

34. L. H. Van Vlack, Physical Ceramics for Engineers, Ann Arbor, Malloy Printing, (1960) 49.

35. M. Hansen, Constitution of Binary Alloys, McGraw-Hill Book Co., New York, (1958).

36. C. E. Roberts, "The Alloys of Aluminum and Silicon," J. Chem. Soc., 105 (2), (1914) 1383.

37. S. Tamaru, "Über die Legierung des Siliciums mit Zinn, Blei, und Thallium," Z. anorg. Chem., 61, (1909) 40.

38. G. Voss, "Die Legierungen: Nickel-Zinn, Nickel-Blei, Nickel-Thallium, Nickel-Wismut, Nickel-Chrom, Nickel-Magnesium, Nickel-Zinn, und Nickel-Cadmium," Z. anorg. Chem., 57, (1908) 52.

39. W. Guertler and A. A. Bergmann, Z. Metallkunde, 25, (1933) 82.

40. M. Kobayashi, "Über die Legierung des Tellurs mit Cadmium and Zinn," Z. anorg. Chem., 69, (1911) 6.

41. G. Grube and R. Bornhak, "Das Zustandsdigramm Magnesium-Antimon," Z. Elektrochem., 40, (1934) 140.

42. W. Koster and B. Thoma, "Aufbau ternarer Systeme von Metallen der dritten und funften Gruppe des Periodischen Systems," Z. Metallkunde, 46, (1955) 291.

43. E. F. Osborn and A. Muan, Phase Equilibrium Diagrams of Oxide Systems, The American Ceramic Soc., Columbus, (1960), Plate 2.

44. R. W. Ricker and E. F. Osborn, "Additional Phase Equilibrium Data for the System CaO - MgO - SiO_2," J. Am. Ceram. Soc., 37, (1954) 133.

45. R. B. Sosmon and Olaf Anderson, Phase Equilibrium Diagrams of the Refractory Oxides, Research Laboratory, U.S. Steel Corp., (1946), Plate 4.

46. G. A. Rankin and H. E. Merwin, "Das Ternare System: Calciumoxyd-Aluminumoxyd-Magnesiumoxyd," Z. Anorg. u. allgem. Chem., 96, (1916) 309.

47. J. R. Rait, "Basic Refractories," Iron and Steel, 23, (1950) 90.

48. A. Taylor, X-Ray Metallography, John Wiley and Sons, New York, (1961) 649.

49. C. Wagner, "Thermodynamics of Phase Diagrams of Binary Systems Involving Compounds," Acta Met, 6, (1958) 309.

50. W. F. Schottky and M. B. Bever, "On The Thermodynamic Properties of the III-V Compounds In Sb, Ga Sb, and In As," Acta Met, 6, (1958) 320.

51. M. R. Kalyanram and H. B. Bell, "Activities in the System CaO-MgO-Al_2O_3," Trans. British Ceram. Soc., 60, (1961) 135.

52. F. D. Richardson, "Oxide Slags - A Survey of Our Present Knowledge," The Physical Chemistry of Steelmaking, Technology Press of MIT and John Wiley and Sons, New York, (1958) 55.